

Adiabatic extraction of nonlinear optical properties from real-time time-dependent electronic-structure theory

Benedicte Sverdrup Ofstad,^{1, a)} Håkon Emil Kristiansen,¹ Einar Aurbakken,¹ Øyvind Sigmundson Schøyen,² Simen Kvaal,¹ and Thomas Bondo Pedersen^{1, b)}

¹⁾*Hylleraas Centre for Quantum Molecular Sciences, Department of Chemistry, University of Oslo, Norway*

²⁾*Department of Physics, University of Oslo, Norway*

(Dated: 7 February 2023)

Real-time simulations of laser-driven electron dynamics contain information about molecular optical properties through all orders in response theory. These properties can be extracted by assuming convergence of the power series expansion of induced electric and magnetic multipole moments. However, the accuracy relative to analytical results from response theory quickly deteriorates for higher-order responses due to the presence of high-frequency oscillations in the induced multipole moment in the time domain. This problem has been ascribed to missing higher-order corrections. We here demonstrate that the deviations are caused by nonadiabatic effects arising from the finite-time ramping from zero to full strength of the external laser field. Three different approaches, two using a ramped wave and one using a pulsed wave, for extracting electrical properties from real-time time-dependent electronic-structure simulations are investigated. The standard linear ramp is compared to a quadratic ramp, which is found to yield highly accurate results for polarizabilities, and first and second hyperpolarizabilities, at roughly half the computational cost. Results for the third hyperpolarizability are presented along with a simple, computable measure of reliability.

I. INTRODUCTION

Extraction of frequency-dependent, off-resonance linear and nonlinear optical properties of molecules from real-time time-dependent electronic-structure simulations has been increasingly used^{1–16} in place of conventional response theory^{17,18} in recent years. One likely reason is that the implementation of response theory becomes increasingly cumbersome with increasing response order, whereas time-dependent methods are relatively straightforward to implement.

While response theory is based on perturbation expansions, real-time approaches where the initial ground-state wave function (or density or density matrix) is propagated in the presence of an external laser field automatically include responses to all orders in perturbation theory. In principle, therefore, optical response properties through *any* order can be extracted from induced multipole moments recorded during the real-time simulation. If the total number of time steps in the wave function propagation can be kept low enough, the real-time approach may become computationally advantageous over the response approach for higher-order nonlinear properties such as the second hyperpolarizability.

The time required for real-time simulations depends on several parameters besides the inherent computational complexity of the equations of motion for the wave function parameters, which generally take the form $\dot{y} = f(y, t)$ where the dot denotes the time derivative. The choice of integrator affects how large a time step

may be used without sacrificing accuracy and the number of expensive evaluations of the function $f(y, t)$ per time step. For given choices of electronic-structure model and suitable integrator, however, the key parameter determining both computational effort and accuracy of the extracted properties is the form used for the external, time-dependent field.

Two general approaches for the extraction of response properties have been proposed recently. While Uemoto *et al.*¹² used a pulsed (i.e., with finite duration) wave, Ding *et al.*⁶ used a monochromatic continuous wave ramped from zero to full strength in a finite-time interval to mimic the adiabatic switching-on required by response theory. In both cases, the individual orders of the response of the electronic system are separated by running simulations with different field strengths, followed by curve fitting to extract specific frequency-dependent properties at each order. The accuracy and total simulation time thus intrinsically depend on the duration of the pulsed or continuous wave, including the ramping time for the latter.

In this work, we investigate the convergence of the extracted response properties (polarizabilities, and first and second hyperpolarizabilities) towards the results from response theory with respect to the duration of the pulsed wave (PW). For the ramped continuous wave (RCW) approach, we perform the same convergence study with respect to the adiabatic ramping time and the post-ramp time.

The results reported by Ding *et al.*⁶ indicate that linear polarizabilities can be extracted from simulations with errors below $\sim 1\%$, while the percentwise errors increase by roughly a factor of ten at each nonlinear order for hyperpolarizabilities. The source of these errors is the significant deviation of the higher-order time-domain

^{a)}Electronic mail: b.s.ofstad@kjemi.uio.no

^{b)}Electronic mail: t.b.pedersen@kjemi.uio.no

dipole signals from the form expected from frequency-dependent response theory. Fig. 1 shows an example for the Ne atom where we have extracted the third-order induced dipole moment from time-dependent coupled-cluster singles-and-doubles (TDCCSD) simulations with the approach recommended by Ding *et al.*⁶ That is, we

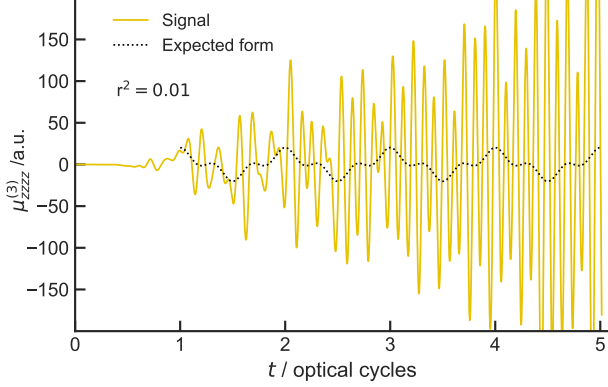


FIG. 1: Comparison of the third-order induced dipole moment extracted from TDCCSD simulations of the Ne atom with a least-squares fitting to the form expected from response theory.

have used a continuous wave linearly ramped for one optical cycle, followed by wave-function propagation with full field strength for four optical cycles. Evidently, the deviation between the computed dipole and the fitted one is much too big for an accurate determination of the second hyperpolarizability, as also indicated by the coefficient of determination, $r^2 = 0.01$.

Such deviations have been ascribed to higher-order truncation errors.⁶ In this work we investigate if the deviations can be reduced by switching to a softer adiabatic ramping, while maintaining or reducing the total computational cost of the time-dependent simulations.

The remainder of the paper is organized as follows. In Sec. II we review the RCW and PW methods for extracting up to the third hyperpolarizability and propose an alternative to the linear ramping of Ding *et al.*⁶ aimed at mitigating nonadiabatic effects. Test systems and other computational details are provided in Sec. III, followed by presentation and discussion of results in Sec. IV. Finally, concluding remarks are given in Sec. V.

II. THEORY

The electronic dynamics induced by an electromagnetic field is governed by the time-dependent Schrödinger equation,

$$i \frac{\partial \Psi(t)}{\partial t} = \hat{H}(t) \Psi(t), \quad \Psi(0) = \Psi_0, \quad (1)$$

where Ψ_0 is the initial condition, here chosen to be the normalized, time-independent ground-state wavefunction. The time-dependent Hamiltonian $\hat{H}(t)$ is given by

$$\hat{H}(t) = \hat{H}_0 + \hat{V}(t), \quad (2)$$

where \hat{H}_0 is the molecular electronic Hamiltonian in the clamped-nuclei Born-Oppenheimer approximation, and the matter-field interaction operator $\hat{V}(t)$ is given in the length-gauge electric-dipole approximation as

$$\hat{V}(t) = -\hat{\mu} \cdot E(t). \quad (3)$$

Here, $\hat{\mu}$ is the electric-dipole operator and $E(t)$ is a uniform classical electric field. The time evolution of the electric-dipole moment is obtained from the explicitly time-propagated wavefunction as

$$\mu(t) = \langle \Psi(t) | \hat{\mu} | \Psi(t) \rangle. \quad (4)$$

Provided the external field is sufficiently weak and adiabatically switched on, each Cartesian coordinate of the time-dependent dipole moment $\mu_i(t)$ can be expanded as a power series in the electric field $E_j(t)$. Separating the electric-field component $E_j(t) = E_j F(t)$ into a constant amplitude E_j and a time-dependent function $F(t)$, $|F(t)| \leq 1$, we may write¹⁹

$$\begin{aligned} \mu_i(t) = & \mu_i^0 + \sum_j \mu_{ij}^{(1)}(t) E_j + \sum_{jk} \mu_{ijk}^{(2)}(t) E_j E_k \\ & + \sum_{jkl} \mu_{ijkl}^{(3)}(t) E_j E_k E_l \\ & + \sum_{jklm} \mu_{ijklm}^{(4)}(t) E_j E_k E_l E_m + \dots \end{aligned} \quad (5)$$

The time-dependent dipole responses $\mu^{(n)}(t)$ can be written either in the time domain or in the frequency domain.

In the time domain, we may write the dipole responses as the convolutions of time-dependent polarizabilities and hyperpolarizabilities with the field factors $F(t)$,¹⁹

$$\mu_{ij}^{(1)}(t) = \int_{-\infty}^{\infty} \alpha_{ij}^{(1)}(t - t_1) F(t_1) dt_1, \quad (6a)$$

$$\mu_{ijk}^{(2)}(t) = \iint_{-\infty}^{\infty} \alpha_{ijk}^{(2)}(t - t_1, t - t_2) F(t_1) F(t_2) dt_1 dt_2, \quad (6b)$$

$$\begin{aligned} \mu_{ijkl}^{(3)}(t) = & \iiint_{-\infty}^{\infty} \alpha_{ijkl}^{(3)}(t - t_1, t - t_2, t - t_3) \\ & \times F(t_1) F(t_2) F(t_3) dt_1 dt_2 dt_3, \end{aligned} \quad (6c)$$

$$\begin{aligned} \mu_{ijklm}^{(4)}(t) = & \iiint \int_{-\infty}^{\infty} \alpha_{ijklm}^{(4)}(t - t_1, t - t_2, t - t_3, t - t_4) \\ & \times F(t_1) F(t_2) F(t_3) F(t_4) dt_1 dt_2 dt_3 dt_4. \end{aligned} \quad (6d)$$

By causality, the time-dependent (hyper-)polarizability tensors $\alpha^{(n)}$ vanish when any of the arguments $t - t_n < 0$.

In the frequency domain, adopting the conventions of response theory,¹⁷

$$\mu_{ij}^{(1)}(t) = \int_{-\infty}^{\infty} \alpha_{ij}(-\omega; \omega) \tilde{F}(\omega) e^{-i\omega t} d\omega, \quad (7a)$$

$$\mu_{ijk}^{(2)}(t) = \frac{1}{2} \int_{-\infty}^{\infty} \int_{-\infty}^{\infty} \beta_{ijk}(-\omega^{(2)}; \omega_1, \omega_2) \times \tilde{F}(\omega_1) \tilde{F}(\omega_2) e^{-i(\omega_1 + \omega_2)t} d\omega_1 d\omega_2, \quad (7b)$$

$$\mu_{ijkl}^{(3)}(t) = \frac{1}{6} \int_{-\infty}^{\infty} \int_{-\infty}^{\infty} \int_{-\infty}^{\infty} \gamma_{ijkl}(-\omega^{(3)}; \omega_1, \omega_2, \omega_3) \times \tilde{F}(\omega_1) \tilde{F}(\omega_2) \tilde{F}(\omega_3) e^{-i(\omega_1 + \omega_2 + \omega_3)t} \times d\omega_1 d\omega_2 d\omega_3, \quad (7c)$$

$$\mu_{ijklm}^{(4)}(t) = \frac{1}{24} \int_{-\infty}^{\infty} \int_{-\infty}^{\infty} \int_{-\infty}^{\infty} \int_{-\infty}^{\infty} \delta_{ijklm}(-\omega^{(4)}; \omega_1, \omega_2, \omega_3, \omega_4) \times \tilde{F}(\omega_1) \tilde{F}(\omega_2) \tilde{F}(\omega_3) \tilde{F}(\omega_4) e^{-i(\omega_1 + \omega_2 + \omega_3 + \omega_4)t} \times d\omega_1 d\omega_2 d\omega_3 d\omega_4, \quad (7d)$$

where $\omega^{(n)} = \omega_1 + \omega_2 + \dots + \omega_n$ and

$$\tilde{F}(\omega) = \frac{1}{2\pi} \int_{-\infty}^{\infty} F(t) e^{i\omega t} dt. \quad (8)$$

Using the notation of [Olsen and Jørgensen](#),¹⁷ the frequency-dependent (hyper-)polarizabilities are the linear and nonlinear response functions,

$$\alpha_{ij}(-\omega; \omega) = -\langle\langle \hat{\mu}_i; \hat{\mu}_j \rangle\rangle_{\omega}, \quad (9a)$$

$$\beta_{ijk}(-\omega^{(2)}; \omega_1, \omega_2) = \langle\langle \hat{\mu}_i; \hat{\mu}_j, \hat{\mu}_k \rangle\rangle_{\omega_1, \omega_2}, \quad (9b)$$

$$\gamma_{ijkl}(-\omega^{(3)}; \omega_1, \omega_2, \omega_3) = -\langle\langle \hat{\mu}_i; \hat{\mu}_j, \hat{\mu}_k, \hat{\mu}_l \rangle\rangle_{\omega_1, \omega_2, \omega_3}, \quad (9c)$$

$$\delta_{ijklm}(-\omega^{(4)}; \omega_1, \omega_2, \omega_3, \omega_4) = \langle\langle \hat{\mu}_i; \hat{\mu}_j, \hat{\mu}_k, \hat{\mu}_l, \hat{\mu}_m \rangle\rangle_{\omega_1, \omega_2, \omega_3, \omega_4}. \quad (9d)$$

The response functions of the right-hand sides can in principle be evaluated analytically with a wide range of quantum chemical methods using response theory,²⁰ although we are not aware of any implementation beyond cubic response—i.e., beyond the second hyperpolarizability γ_{ijkl} .

With the electric field polarized along a specific axis, say j , the “diagonal” components of the dipole responses, $\mu_{ijj\dots j}^{(n)}(t)$, can be extracted from $\mu_i(t)$ recorded during

simulations using the central difference formulas,

$$\mu_{ij}^{(1)}(t) \approx \frac{8\Delta_i^-(t, E_j) - \Delta_i^-(t, 2E_j)}{12E_j}, \quad (10a)$$

$$\mu_{ijj}^{(2)}(t) \approx \frac{16\Delta_i^+(t, E_j) - \Delta_i^+(t, 2E_j) - 30\mu_i^0}{24E_j^2}, \quad (10b)$$

$$\mu_{ijjj}^{(3)}(t) \approx \frac{-13\Delta_i^-(t, E_j) + 8\Delta_i^-(t, 2E_j) - \Delta_i^-(t, 3E_j)}{48E_j^3}, \quad (10c)$$

$$\mu_{ijjjj}^{(4)}(t) \approx \frac{1}{144E_j^4} \left(-39\Delta_i^+(t, E_j) + 12\Delta_i^+(t, 2E_j) - \Delta_i^+(t, 3E_j) + 56\mu_i^0 \right). \quad (10d)$$

The truncation error is $\mathcal{O}(E_j^4)$ in each case, and

$$\Delta_i^{\pm}(t, E_j) = \mu_i(t, E_j) \pm \mu_i(t, -E_j), \quad (11)$$

is the sum/difference of the time-dependent dipole moments computed with opposite polarization directions and same field strength E_j . One can now use different choices for $F(t)$ to obtain the frequency-dependent response functions, using either the frequency-domain expressions (7) or those in the time-domain (6).

A. Ramped continuous wave approach

As the name suggests, the RCW approach uses a continuous wave, i.e., $F(t) = \cos(\omega t)$. This choice allows us to perform the Fourier transformations of Eq. (7) analytically to obtain

$$\mu_{ij}^{(1)}(t) = \alpha_{ij}(-\omega; \omega) \cos(\omega t), \quad (12a)$$

$$\mu_{ijj}^{(2)}(t) = \frac{1}{4} [\beta_{ijj}^{\text{SHG}}(\omega) \cos(2\omega t) + \beta_{ijj}^{\text{OR}}(\omega)], \quad (12b)$$

$$\mu_{ijjj}^{(3)}(t) = \frac{1}{24} [\gamma_{ijjj}^{\text{THG}}(\omega) \cos(3\omega t) + 3\gamma_{ijjj}^{\text{DFWM}}(\omega) \cos(\omega t)], \quad (12c)$$

$$\mu_{ijjjj}^{(4)}(t) = \frac{1}{192} [\delta_{ijjjj}^{\text{FHG}}(\omega) \cos(4\omega t) + 4\delta_{ijjjj}^{\text{FSHG}}(\omega) \cos(2\omega t) + 3\delta_{ijjjj}^{\text{HOR}}(\omega)], \quad (12d)$$

where the (hyper-)polarizabilities are assumed real, a valid assumption given that \hat{H}_0 does not contain static

magnetic fields, and

$$\beta_{ijj}^{\text{SHG}}(\omega) = \beta_{ijj}(-2\omega, \omega, \omega), \quad (13a)$$

$$\beta_{ijj}^{\text{OR}}(\omega) = \beta_{ijj}(0, \omega, -\omega), \quad (13b)$$

$$\gamma_{ijjj}^{\text{THG}}(\omega) = \gamma_{ijjj}(-3\omega; \omega, \omega, \omega), \quad (13c)$$

$$\gamma_{ijjj}^{\text{DFWM}}(\omega) = \gamma_{ijjj}(-\omega; \omega, \omega, -\omega), \quad (13d)$$

$$\delta_{ijjjj}^{\text{FHG}}(\omega) = \delta_{ijjjj}(-4\omega; \omega, \omega, \omega, \omega), \quad (13e)$$

$$\delta_{ijjjj}^{\text{HSHG}}(\omega) = \delta_{ijjjj}(-2\omega; \omega, \omega, \omega, -\omega), \quad (13f)$$

$$\delta_{ijjjj}^{\text{HOR}}(\omega) = \delta_{ijjjj}(0; \omega, \omega, -\omega, -\omega). \quad (13g)$$

The superscripts refer to the following nonlinear optical processes: Second harmonic generation (SHG), optical rectification (OR), third harmonic generation (THG), degenerate four-wave mixing (DFWM), fourth harmonic generation (FHG), higher-order second harmonic generation (HSHG), and higher-order optical rectification (HOR). With the left-hand sides known from simulations through Eqs. (10), the Eqs. (12) yield the frequency-dependent (hyper-)polarizabilities by curve fitting.

Frequency-dependent response theory, however, requires the field to be adiabatically switched on.¹⁷ This can be achieved by a smooth modification of the continuous wave such that it is switched-on at $t \rightarrow -\infty$ and reaches full strength at $t \rightarrow \infty$. Of course, this is impractical and a finite-time ramping of the field from zero to full strength must be applied in a way that minimizes nonadiabatic effects, using only post-ramp signals to extract the dipole responses $\mu^{(n)}(t)$. In Ref. 6, the adiabatic switching-on is simulated by a linear ramp lasting for one optical cycle, i.e., a ramping time $t_r = t_c$ where the cycle time is $t_c = \frac{2\pi}{\omega}$. We refer to this approach as the linear RCW (LRCW) approach for which

$$F^{\text{LRCW}}(t) = \begin{cases} \frac{t}{t_r} \cos(\omega t) & 0 \leq t < t_r \\ \cos(\omega t) & t_r \leq t \leq t_{\text{tot}}. \end{cases} \quad (14)$$

Following the ramping phase, Ding *et al.*⁶ propagated the system for a further four optical cycles, giving a total simulation time of $t_{\text{tot}} = 5t_c$. We will here investigate the effect of a longer ramping time consisting of n_r optical cycles, $t_r = n_r t_c$. We note that the linear ramp is not continuously differentiable at $t = 0$ and at $t = t_r$.

In addition to extending the ramping time beyond a single optical cycle, we investigate the *quadratic ramp* to achieve a more adiabatic switching on of the electric field. We refer to this approach as the quadratic RCW (QRCW) approach. Specifically,

$$F^{\text{QRCW}}(t) = \begin{cases} \frac{2t^2}{t_r^2} \cos(\omega t) & 0 \leq t < \frac{t_r}{2} \\ \frac{t_r^2 - 2(t - t_r)^2}{t_r^2} \cos(\omega t) & \frac{t_r}{2} \leq t < t_r \\ \cos(\omega t) & t_r \leq t \leq t_{\text{tot}} \end{cases} \quad (15)$$

which is continuously differentiable at both $t = 0$ and $t = t_r$. As illustrated in Fig. 2, the quadratic ramp provides a gentler increase of the electric field than the lin-

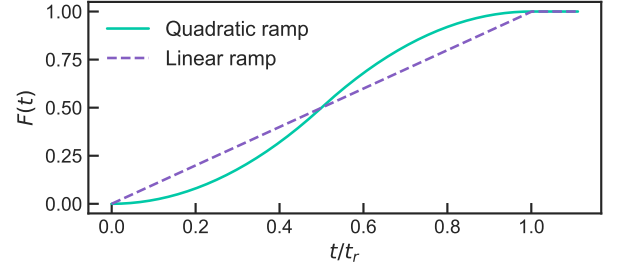


FIG. 2: The time profiles F^{LRCW} and F^{QRCW} with $\omega = 0$.

ear ramp for small t and near $t = t_r$, albeit with a more rapid increase around $t = \frac{t_r}{2}$. A similar sigmoid (Fermi-like) function has been used to obtain electronic ground states by adiabatically switching on electronic interactions, thus providing an alternative to imaginary-time propagation.²¹

B. Pulsed wave approach

Uemoto *et al.*¹² proposed an alternative approach to the extraction of linear and nonlinear properties from simulations of electron dynamics driven by a laser pulse rather than by a continuous wave. We refer to this approach as the pulsed wave (PW) approach, which starts from the time-domain responses, Eqs. (6). Retardation effects are neglected and the polarization thus is considered local in time, i.e.,

$$\begin{aligned} \mu^{(n)}(t) &= \iint \dots \int_{-\infty}^{\infty} \alpha^{(n)}(t - t_1, t - t_2, \dots, t - t_n) \\ &\quad \times F(t_1)F(t_2) \dots F(t_n) dt_1 dt_2 \dots dt_n \\ &\approx \alpha^{(n)}(t) F(t)^n, \end{aligned} \quad (16)$$

where the cartesian indices have been omitted for notational convenience. Following Uemoto *et al.*,¹² the time-dependence of the finite laser pulse is described using a trigonometric envelope, which provides a well-defined approximation to the gaussian envelope typically used in experimental work,²²

$$F^{\text{PW}}(t) = \sin^2\left(\frac{\pi t}{t_{\text{tot}}}\right) \cos(\omega t), \quad 0 \leq t \leq t_{\text{tot}}. \quad (17)$$

The finite duration of the laser pulse implies that the frequency distribution is broadened around the carrier frequency ω . This, in turn, implies that $\alpha^{(n)}(t)$ contains (hyper-)polarizabilities in a range of frequencies and, therefore, a filtering procedure must be applied to extract the proper nonlinear response functions in the frequency domain. If the frequency distribution of the laser pulse is sufficiently sharply centered at the carrier frequency—i.e., if the pulse duration is sufficiently long—

the linear polarizability dominates the time signal and can be found by a direct fitting of the signal to the time profile of the pulse,

$$\mu_{ij}^{(1)}(t) = \alpha_{ij}(-\omega; \omega) F^{\text{PW}}(t). \quad (18)$$

This is essentially the same procedure used for a monochromatic continuous wave, Eq. (12a), above.

For the hyperpolarizabilities, where more than one frequency component is present in the signal, the individual frequency components are separated by means of a Fourier filtering procedure: $\mu^{(n)}(t)$ is Fourier transformed to the frequency domain to obtain

$$\tilde{\mu}^{(n)}(\omega') = \frac{1}{2\pi} \int_{-\infty}^{\infty} \mu^{(n)}(t) e^{i\omega' t} dt, \quad (19)$$

which is subsequently transformed back to the time domain using a suitably chosen frequency window specified as a positive integer multiple k of the carrier frequency ω :

$$\begin{aligned} \mu^{(n)}(t; k\omega) &= \int_{-(k+1)\omega}^{-(k-1)\omega} \tilde{\mu}^{(n)}(\omega') e^{-i\omega' t} d\omega' \\ &+ \int_{(k-1)\omega}^{(k+1)\omega} \tilde{\mu}^{(n)}(\omega') e^{-i\omega' t} d\omega'. \end{aligned} \quad (20)$$

The same procedure is applied to $F^{\text{PW}}(t)$:

$$\begin{aligned} F^{\text{PW}}(t; k\omega) &= \int_{-(k+1)\omega}^{-(k-1)\omega} \tilde{F}^{\text{PW}}(\omega') e^{-i\omega' t} d\omega' \\ &+ \int_{(k-1)\omega}^{(k+1)\omega} \tilde{F}^{\text{PW}}(\omega') e^{-i\omega' t} d\omega', \end{aligned} \quad (21)$$

The frequency-dependent hyperpolarizabilities are then acquired by finding the coefficient needed to fit $\mu^{(n)}(t; k\omega)$ to $[F^{\text{PW}}(t; k\omega)]^n$. Thus, the first hyperpolarizabilities are found by curve fitting according to

$$\mu_{ijj}^{(2)}(t; 0) = \frac{1}{4} \beta_{ijj}^{\text{OR}}(\omega) [F^{\text{PW}}(t; 0)]^2, \quad (22a)$$

$$\mu_{ijj}^{(2)}(t; 2\omega) = \frac{1}{4} \beta_{ijj}^{\text{SHG}}(\omega) [F^{\text{PW}}(t; 2\omega)]^2, \quad (22b)$$

the second hyperpolarizabilities according to

$$\mu_{ijjj}^{(3)}(t; \omega) = \frac{1}{8} \gamma_{ijjj}^{\text{DFWM}}(\omega) [F^{\text{PW}}(t; \omega)]^3, \quad (23a)$$

$$\mu_{ijjj}^{(3)}(t; 3\omega) = \frac{1}{24} \gamma_{ijjj}^{\text{THG}}(\omega) [F^{\text{PW}}(t; 3\omega)]^3, \quad (23b)$$

and the third hyperpolarizabilities according to

$$\mu_{ijjjj}^{(4)}(t; 0) = \frac{1}{64} \delta_{ijjjj}^{\text{HOR}}(\omega) [F^{\text{PW}}(t; 0)]^4, \quad (24a)$$

$$\mu_{ijjjj}^{(4)}(t; 2\omega) = \frac{1}{48} \delta_{ijjjj}^{\text{HSHG}}(\omega) [F^{\text{PW}}(t; 2\omega)]^4, \quad (24b)$$

$$\mu_{ijjjj}^{(4)}(t; 4\omega) = \frac{1}{192} \delta_{ijjjj}^{\text{FHHG}}(\omega) [F^{\text{PW}}(t; 4\omega)]^4. \quad (24c)$$

III. COMPUTATIONAL DETAILS

The time-dependent Schrödinger equation (1) is solved approximately using the time-dependent configuration-interaction singles (TDCIS)^{23,24} method, the time-dependent coupled-cluster singles-and-doubles (TD-CCSD)²⁵ method, the second-order approximate time-dependent coupled-cluster (TDCC2)^{15,26} model, and the time-dependent orbital-optimized second-order Møller-Plesset (TDOMP2)^{15,27} model. For the nonvariational methods, the dipole moment is computed using the inherently real expectation-value functional proposed in Refs. 25 and 28.

We test the RCW and PW approaches using the same ten-electron systems as in Ref. 15, namely Ne, HF, H₂O, NH₃, and CH₄. The geometries of these molecules can be found in the supplementary material. The d-aug-cc-pVDZ²⁹ basis set is used for Ne, while the aug-cc-pVDZ³⁰ basis set is used for the four remaining systems. The basis set definitions are taken from the Basis Set Exchange.³¹ The carrier frequencies are chosen in accord with Ref. 15: Ne: $\omega = 0.1$, HF: $\omega = 0.1$, H₂O: $\omega = 0.0428$, NH₃: $\omega = 0.0428$, and CH₄: $\omega = 0.0656$ a.u. These frequencies come in at less than one third of the first dipole-allowed excitation energy for each system, enabling properties up to (at least) the third hyperpolarizability to be reliably extracted.

The Hartree-Fock reference orbitals and Hamiltonian integrals are calculated using the Python-based Simulations of Chemistry Framework³² (PySCF) with the gradient norm convergence threshold set to 10^{-10} a.u.

The ground states are computed using a locally developed closed-shell spin-restricted code³³, all computed with a residual norm convergence criteria of 10^{-12} a.u. The equations of motion are integrated using the sixth order (three-stage, $s = 3$) symplectic Gauss-Legendre integrator³⁴ as described in Ref. 25 with a time step of $\Delta t = 0.01$ a.u. and the residual norm convergence criterion set to 10^{-10} a.u. for the implicit equations. The least-squares curve fitting, using the Levenberg-Marquardt algorithm, as implemented in the *optimize* module of SciPy³⁵ is used to extract the (hyper-)polarizabilities.

The coupled-cluster response data are computed using the Dalton quantum chemistry package³⁶⁻⁴² with the following gradient/residual norm convergence criteria: 10^{-10} a.u. for the Hartree-Fock reference orbitals, 10^{-10} a.u. for the CC ground-state residual norms, and 10^{-8} a.u. for the response equations. The CIS re-

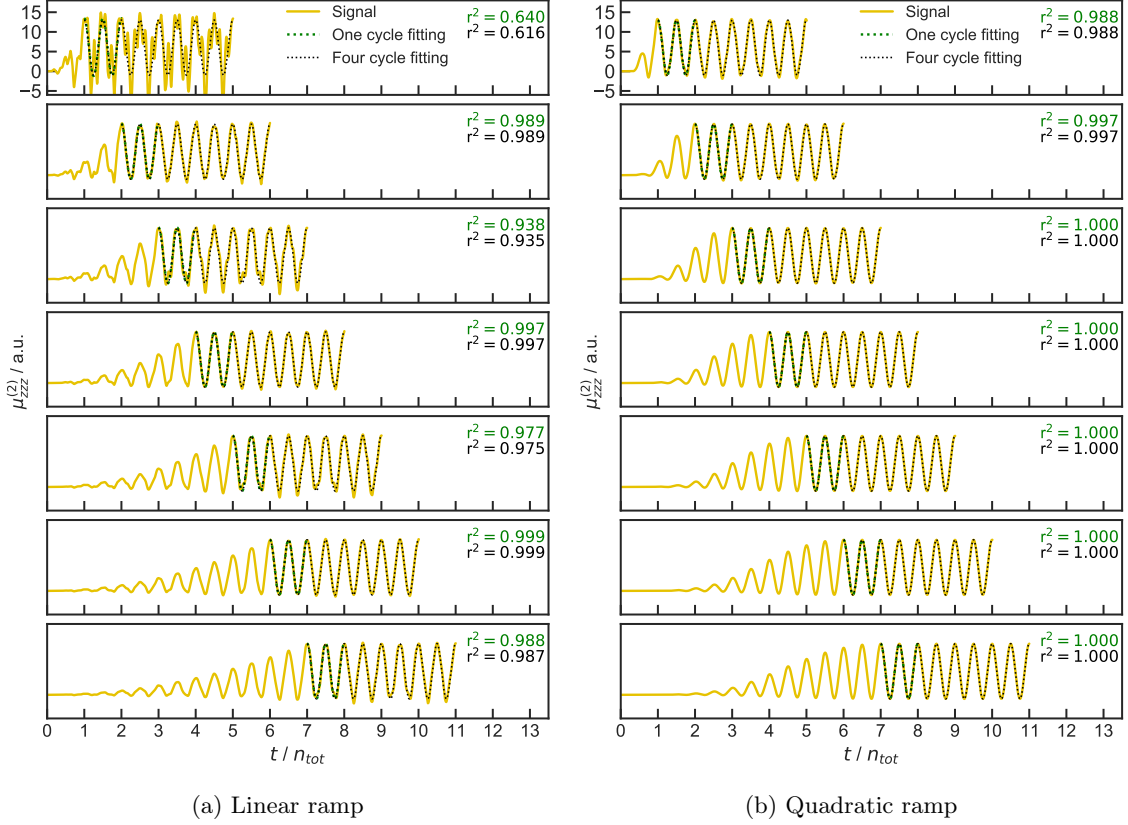


FIG. 3: The second-order dipole response obtained from TDCCSD simulations using, from top to bottom, $n_r = (1, 2, 3, 4, 5, 6, 7)$ linear ramp (a) or quadratic ramp (b) cycles followed by four post-ramp cycles of propagation time for NH_3 . The fitting in black is done on all four post-ramp cycles, the fitting in green is done on one post-ramp cycle. All plots are on the same scale.

sponse data are computed using sum-over-states expressions.^{17,43}

For all simulations, the electric-field strengths $E = \pm 0.001, \pm 0.002, \pm 0.003$ a.u. are used in order to reduce numerical noise for higher-order properties. The electric-field strengths should be of a magnitude where *both* the errors associated with numerical noise *and* the errors arising from numerical truncation and nonadiabatic effects remain small. Ding *et al.*⁶ explored field strengths in the range 0.0005 a.u. to 0.005 a.u. and found $E = 0.002$ a.u. to provide the most accurate results. Uemoto *et al.*¹² used field strengths from $E \approx 0.0002$ a.u. to $E \approx 0.002$ a.u., and did not find the PW approach to be sensitive within this range.

IV. RESULTS

A. Time evolution of the nonlinear dipole responses in the RCW approach

The accuracy of the (hyper-)polarizabilities obtained using the RCW approach depends on how closely the time-domain dipole responses $\mu^{(n)}(t)$ *actually* are to their

expected forms, expressed by Eqs. (12a) – (12d). Therefore, we start by comparing the signals extracted after linear and quadratic ramping. The motivation for this is twofold: Firstly, we wish to investigate if the deviations previously observed⁶ for time signals of nonlinear properties can be alleviated with the closer-to-adiabatic quadratic ramp. Secondly, we wish to investigate the effect of varying the ramping time $t_r = n_r t_c$ and the propagation time $t_p = n_p t_c$. Their relative importance will be assessed, and the most favorable ratio between n_r and n_p will be determined. When the time parameters are explicitly specified, the approach will be denoted RCW(n_r, n_p). Results obtained with the TDCCSD method will be presented and discussed; analogous results with the TDCC2, TDOMP2, and TDCIS methods are given in the supplementary material.

The systems are ramped using either the linear ramp profile F^{LRCW} [Eq. (14)] or the quadratic ramp profile F^{QRCW} [Eq. (15)]. The ramp duration is increased in increments of one optical cycle, up to a maximum of seven optical cycles ($n_r = 1, 2, \dots, 7$), followed by four optical cycles of propagation ($n_p = 4$). The second- and third-order time-dependent dipole responses $\mu^{(n)}(t)$, $n = 2, 3$, are collected, and fitted to the expected shapes

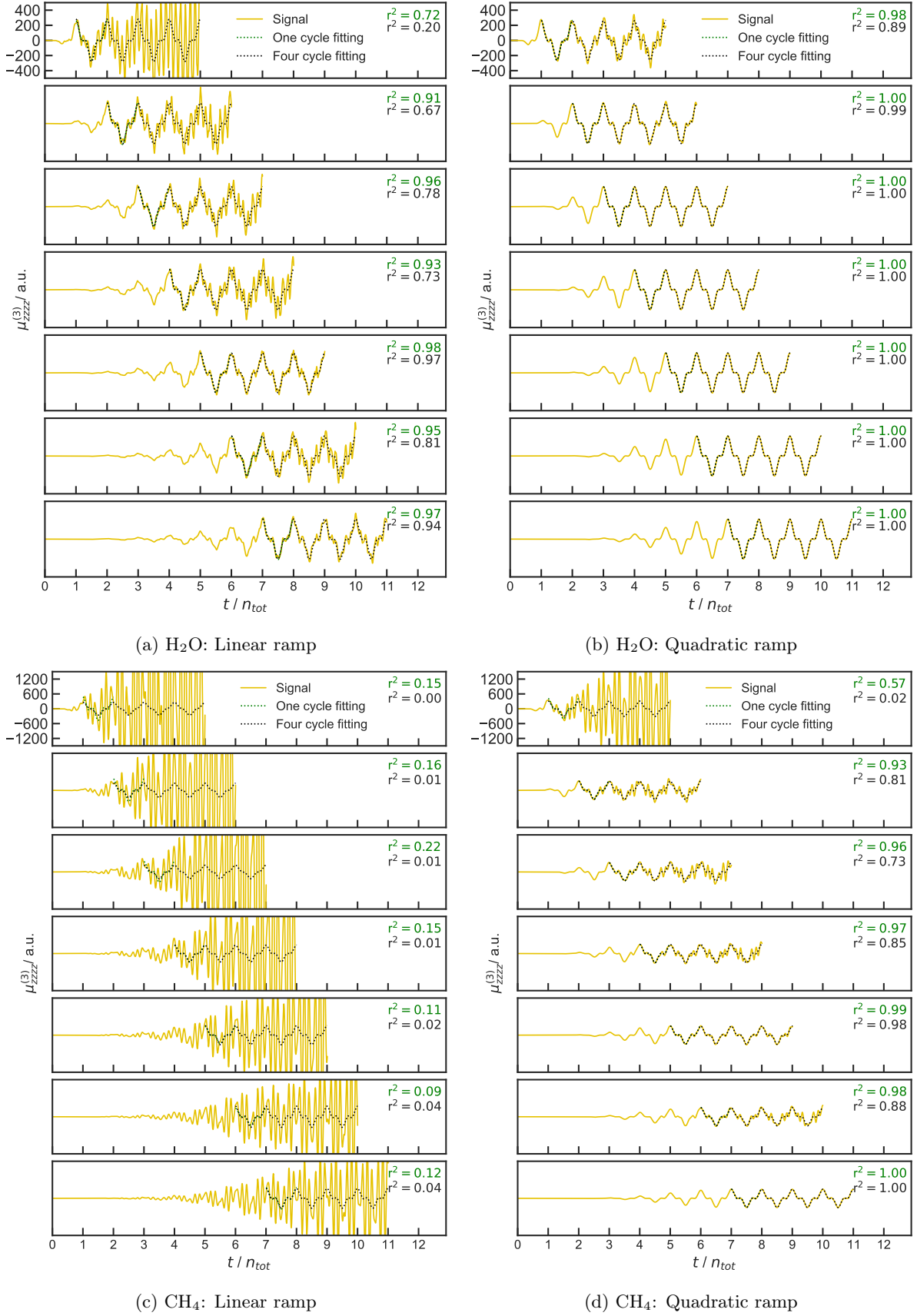


FIG. 4: The third-order dipole response obtained from TDCCSD simulations using, from top to bottom, $n_r = (1, 2, 3, 4, 5, 6, 7)$ linear ramp (a) or quadratic ramp (b) cycles followed by four post-ramp cycles of propagation for H_2O and Ne . The fitting in black is done on all four post-ramp cycles, the fitting in green is done on one post-ramp cycle. All four plots are on the same scale for each system.

in Eqs. (12b) and (12c).

The time-domain dipole response $\mu_{zzz}^{(2)}(t)$ for the NH_3 molecule is displayed in Fig. 3. The upper-most panel exhibits the one-cycle ramp, and for each descending panel the number of ramping cycles is increased by one. The function obtained by fitting the analytic form over the range of four cycles post-ramp is displayed in black along with its coefficient of determination, r^2 . The function obtained by fitting to one post-ramp cycle is plotted in green.

Ramping with the linear profile, we observe the high-frequency oscillations previously reported in Refs. 6 and 15. The correspondence between the signal and expected form improves significantly as the linear ramping time is increased to two and three optical cycles. Increasing the linear ramp time above three optical cycles only delivers marginal improvements. The simulations conducted using the quadratic ramp, in contrast, appear to behave correctly already at the one-cycle ramp stage. Evidently, the signal can be improved either by switching to the quadratic ramp or by increasing the duration of the linear ramping. The curves fitted using one post-ramp cycle typically have r^2 values slightly above those obtained by fitting to four post-ramp cycles.

The second hyperpolarizability, a much smaller contribution to the total induced dipole moment, is highly sensitive to errors in the time signal. The third-order response signal, $\mu_{zzz}^{(3)}(t)$, features both the high-frequency oscillations observed for the first hyperpolarizability and the increase of amplitude as time progresses. The molecule least sensitive to these effects is H_2O , for which results are presented in Fig. 4a–4b. The molecule most sensitive is CH_4 , for which results are presented in Fig. 4c–4d. The linear one-cycle ramp is clearly inadequate for describing the second hyperpolarizability for both molecules, indicating that even a small amount of nonadiabatic error dramatically reduces the correspondence of the signal with its expected form. Increasing the ramping time to two or three optical cycles greatly improves the signal, but analogously to what was observed for the first hyperpolarizability, increasing beyond three cycles does not improve the signal. Even with increased ramping time, the linear ramp does not provide an accurate description of the third order response signal, yielding at best $r^2 = 0.22$ for CH_4 . The quadratic ramp profile fares notably better, although the high-frequency oscillations and the drift of the amplitude is observed for the CH_4 molecule when a one-cycle ramp is employed—i.e., in contrast to what was observed for the first hyperpolarizability, a one-cycle quadratic ramp appears to be insufficient. Increasing the number of ramping cycles quickly leads to convergence, giving $r^2 = 0.99998$ when seven cycles are used for the CH_4 molecule.

The gradual ramping of the electric-field strength is found to reduce the signal errors indicating that nonadiabatic effects are the main source of error, not higher-order response contributions. Furthermore, it is clear that the quadratic ramp aids in reaching an adiabatic description

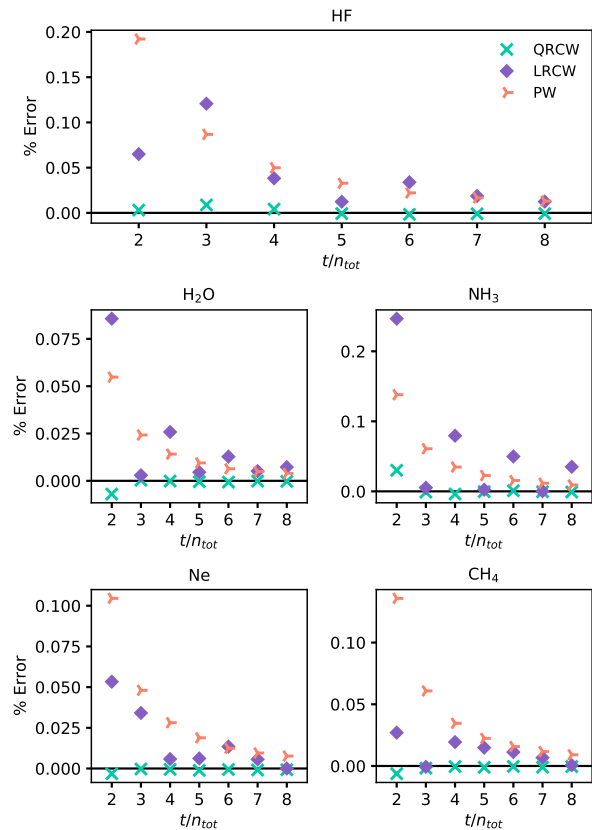


FIG. 5: Convergence towards CCSD linear response results of polarizabilities, α_{zz} , extracted from TDCCSD simulations using the LRCW($n_{\text{tot}} - 1, 1$), QRCW($n_{\text{tot}} - 1, 1$), and PW(n_{tot}) methods.

more rapidly than the linear ramp. It is found that fitting the expected function to the signal after only one post-ramp cycle is warranted when the simulation has ramped in a sufficiently adiabatic manner. Based on these observations, we shall compare the RCW method to the PW method using one post-ramp cycle.

B. Polarizability

In the interest of gauging the accuracy of the different approaches, polarizabilities extracted using the LRCW, QRCW, and PW approach are compared to response theory calculations. By assessing the closeness of the real-time approaches to response theory at different total simulation times, $t_{\text{tot}} = (n_r + n_p)t_c = n_{\text{tot}}t_c$, we may compare the accuracy achieved by the three approaches at similar computational costs.

The RCW simulations are performed using $n_{\text{tot}} = n_r + 1$, i.e., using the LRCW($n_r, 1$) and QRCW($n_r, 1$) methods, in line with the discussion in section IV A. The first-order dipole response is separated from the time signal using the finite difference formula (10) for all approaches. By point-group symmetry, the polarizability

TABLE I: First hyperpolarizabilities, β_{zzz}^{SHG} , extracted from TDCCSD simulations using the LRCW(n_r, n_p) and QRCW(n_r, n_p) methods compared with CCSD linear response results.

	HF	H ₂ O	NH ₃
LRCW(1,4)	14.428	-9.683	29.330
QRCW(1,4)	14.372	-9.588	28.022
QRCW(1,1)	14.375	-9.603	27.941
QRCW(2,1)	14.368	-9.590	28.005
QRCW(3,1)	14.371	-9.590	28.027
QRCW(4,1)	14.372	-9.591	28.020
QRCW(5,1)	14.370	-9.591	28.020
Response	14.370	-9.591	28.020

tensors of Ne and CH₄ are equal for all Cartesian directions, and only the zz component is computed. For the NH₃ and HF molecules, the xx and yy polarizability components are the same by symmetry, whereas polarizability tensors for all three Cartesian directions are computed for H₂O. The polarizabilities at the CCSD level for the five systems in the zz direction are displayed in Fig. 5. The other unique polarizability components at the CCSD level can be found in the supplementary material along with CC2 results.

The QRCW approach consistently produces polarizabilities with the highest accuracy, achieving a 0.03% accuracy after the minimum two cycles of total simulation time, $n_r = 1, n_p = 1$. The PW approach requires longer computational time in order to attain polarizabilities of the same accuracy as QRCW, yet it converges consistently towards the correct value with increasing cycles of simulation time. Albeit with irregular convergence behavior, the LRCW method achieves accuracies comparable to the PW approach as illustrated for the NH₃ and H₂O molecules in Fig. 5.

The errors for the extracted polarizabilities are overall small for all three approaches regardless of ramping. For the shortest ramp length and poorest performing extraction approach, the polarizability is still correct to 0.25%. This modest error can be reduced to below 0.0009% using the QRCW(7,1) method for all molecules.

C. First hyperpolarizability

The second-order dipole response signal is sensitive to nonadiabatic effects, as seen in Fig. 3. Adiabatic ramping, therefore, is expected to significantly improve accuracy.

Due to symmetry, all the diagonal components of the first hyperpolarizability are zero for the Ne and CH₄ molecules. The H₂O and the HF molecule exhibit diagonal first hyperpolarizabilities in the zzz -direction, and the NH₃ molecule has non-vanishing hyperpolarizabilities in the yyy - and zzz -direction. The β_{zzz}^{SHG} and β_{zzz}^{OR} com-

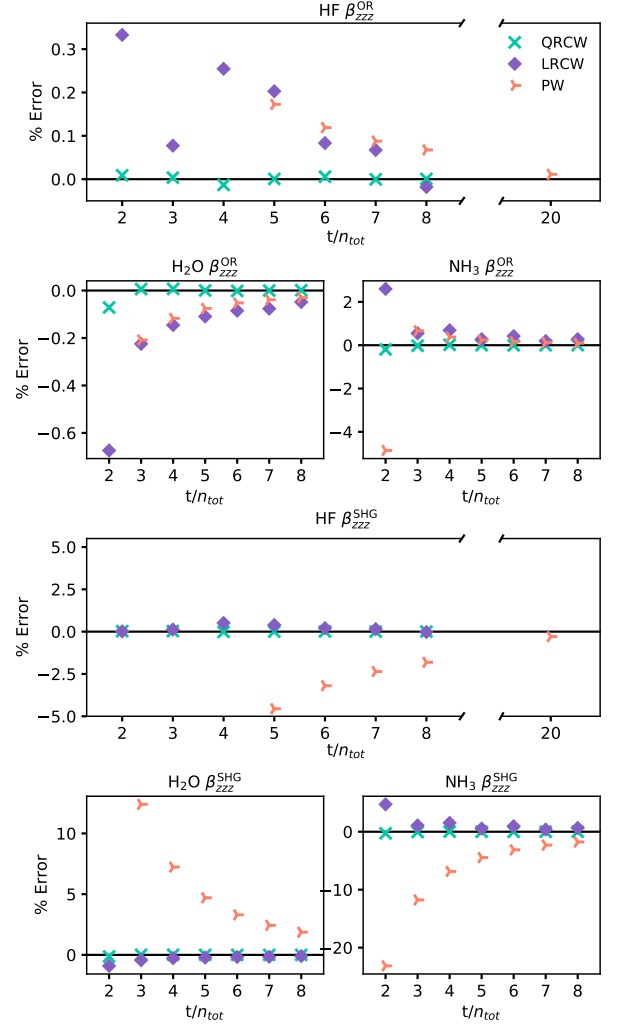


FIG. 6: Convergence towards CCSD quadratic response results of first hyperpolarizabilities extracted from TDCCSD simulations using the LRCW($n_{\text{tot}} - 1, 1$), QRCW($n_{\text{tot}} - 1, 1$), and PW(n_{tot}) methods.

ponents extracted from TDCCSD simulations are displayed in Fig. 6. The β_{yyy}^{SHG} and β_{yyy}^{OR} components of NH₃ can be found in the supplementary material along with all non-zero diagonal first hyperpolarizabilities at the CC2 level.

The errors of the extracted first hyperpolarizabilities are found to be roughly an order of magnitude greater than for polarizabilities with $n_{\text{tot}} = 2$. Using the LRCW(1,1) method to extract the β_{zzz}^{SHG} component yields the following % errors: HF 0.33%, H₂O 0.33%, and NH₃ 2.6%. Using the QRCW(1,1) method reduces these to: HF 0.01%, H₂O 0.07%, NH₃ 0.2%. We obtain hyperpolarizabilities with the smallest relative errors when applying QRCW(7,1) with accuracies of: HF 0.0006%, H₂O 0.001%, NH₃ 0.003% for the β_{zzz}^{SHG} component and: HF 0.003%, H₂O 0.002%, NH₃ 0.005% for the β_{zzz}^{OR} component. With this error reduction the first hyperpolar-

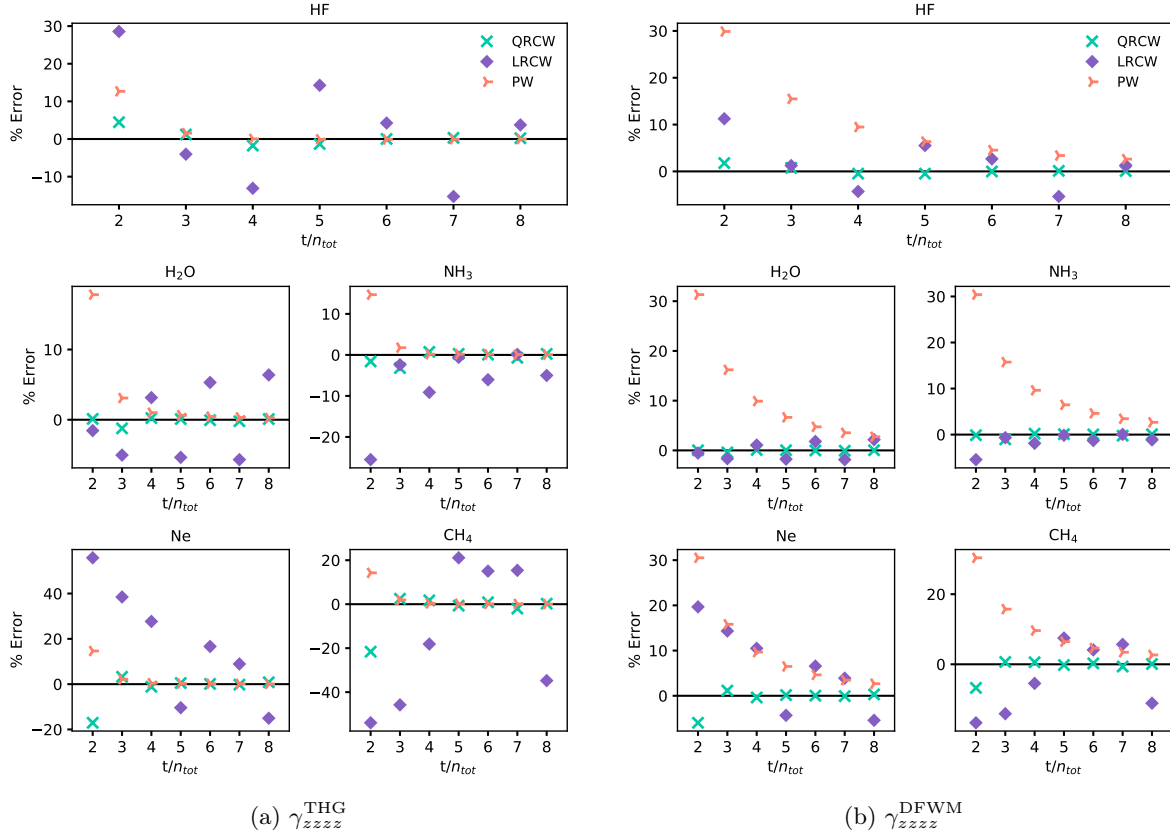


FIG. 7: Convergence towards CCSD cubic response results of second hyperpolarizabilities extracted from TDCCSD simulations using the LRCW($n_{\text{tot}} - 1, 1$), QRCW($n_{\text{tot}} - 1, 1$), and PW(n_{tot}) methods.

izabiliy tensors have accuracies comparable to the extracted polarizability tensors.

The PW approach performs surprisingly poorly with regards to extracting the first hyperpolarizabilities as seen in Fig. 6. For the shortest simulation times, some of the errors obtained for the β_{zzz}^{SHG} component are beyond the scale of the plot, especially for the HF molecule. To check convergence, the total propagation time for the HF molecule was increased to PW(20), resulting in a reduction of the error from 0.07% to 0.01% for the β_{zzz}^{OR} component and from -1.8% to 0.29% for the β_{zzz}^{SHG} component. Although improved, the PW(20) results are still of significantly lower accuracy than the RCW(7,1) results, for which the errors are 0.0006% for the β_{zzz}^{OR} component and 0.004% for the β_{zzz}^{SHG} component.

The accuracies achieved using the QRCW($n_r, 1$) with $n_r = (1, 2, 3, 4, 5)$ are compared to LRCW(1,4) and QRCW(1,4) in Table I. Depending on the demands placed on computational cost and accuracy, it is worth noting that propagating for only two optical cycles ($n_r = n_p = 1$) may be sufficient: The QRCW(1,1) approach produces higher accuracy than the LRCW(1,4) approach.

The errors of the first hyperpolarizabilities presented in this section can be compared with the goodnesses of fit (r^2) of the signals they were extracted from. Taking NH_3

as an example, increasing n_r from 1 to 7 yields the errors (4.68, 1.08, 1.50, 0.53, 0.93, 0.34, 0.65)% with the LRCW method. As expected, the errors correlate strongly to the coefficient of determination of the signal they were extracted from; the r^2 value increases as (0.640, 0.989, 0.938, 0.997, 0.977, 0.999, 0.988). This correlation holds true for all molecules, confirming that the r^2 value can be used as a crude indicator of accuracy.

D. Second hyperpolarizability

Accurate extraction of second hyperpolarizabilities is well known to be challenging, showing errors an order of magnitude greater than those observed for the first hyperpolarizabilities.⁶ An increase of the r^2 values in the third-order dipole response signal will thus substantially increase trust in second hyperpolarizabilities extracted from real-time simulations.

The errors of the $\gamma_{zzzz}^{\text{THG}}$ components as functions of simulation time are compared for the different approaches in Fig. 7a at the CCSD level. Results for the other Cartesian components can be found in the supplementary material, including results obtained from simulations at other levels of theory.

TABLE II: The third harmonic generation components $\gamma_{jjjj}^{\text{THG}}$ of the second hyperpolarizabilities of Ne, HF, H₂O, NH₃ and CH₄ extracted from TDCCSD, TDOMP2, TDCC2, and TDCIS simulations compared with results from cubic response theory.

TDCCSD TDOMP2 TDCC2 TDCIS					TDCCSD TDOMP2 TDCC2 TDCIS						
HF		$\gamma_{xxxx}^{\text{THG}}$					$\gamma_{zzzz}^{\text{THG}}$				
	PW(3)	-718	-912	-1180	-236		-509	-531	-685	-329	
	LRCW(2,1)	-834	-997	-1050	-196		-539	-426	-588	-321	
	QRCW(2,1)	-570	-700	-1010	-227		-511	-524	-643	-332	
	Response	-625		-949	-230		-517		-653	-332	
NH ₃		$\gamma_{yyyy}^{\text{THG}}$					$\gamma_{zzzz}^{\text{THG}}$				
	PW(3)	-1180	-1260	-1380	10.3		-7710	-8930	-9770	-4030	
	LRCW(2,1)	-770	-1850	-2010	-470		-8030	-9500	-11000	-4310	
	QRCW(2,1)	-1260	-1300	-1450	-2.40		-8100	-9070	-9990	-4110	
	Response	-1220		-1420	13.8		-7850		-9950	-4130	
H ₂ O		$\gamma_{xxxx}^{\text{THG}}$					$\gamma_{yyyy}^{\text{THG}}$				
	PW(3)	-1750	-2000	-2320	-796		-546	-562	-653	-14.1	
	LRCW(2,1)	-1980	-1930	-2390	-866		-475	-1040	-766	-174	
	QRCW(2,1)	-1820	-2050	-2380	-831		-559	-584	-668	-23.2	
	Response	-1800		-2380	-820		-565		-675	-13.8	
		$\gamma_{zzzz}^{\text{THG}}$									
	PW(3)	-1040	-1150	-1320	-469						
	LRCW(2,1)	-1130	-1050	-1310	-531						
	QRCW(2,1)	-1090	-1180	-1360	-491						
	Response	-1080		-1360	-483						
Ne		$\gamma_{jjjj}^{\text{THG}}$				CH ₄	$\gamma_{jjjj}^{\text{THG}}$				
	PW(3)	-119	-129	-148	-61.3			-2670	-2750	-2910	19.2
	LRCW(2,1)	-74.6	-189	-120	-63.5			-3950	-3020	-4140	-720
	QRCW(2,1)	-118	-128	-153	-65.5			-2650	-2800	-2910	2.03
	Response	-122		-151	-62.8			-2720		-2960	46.0

Starting with two cycles of simulation time, the LRCW(1,1) approach produces $\gamma_{zzzz}^{\text{THG}}$ results with errors that vary greatly between the systems, spanning from -1.5% for H₂O to +56% for Ne. Increasing the ramping time to seven optical cycles (LRCW(7,1)) does not reduce the errors which now range from -34% for CH₄ to -16% for Ne. The lacking improvement highlights the convergence issues of the LRCW approach, as is clearly visible in the CH₄ and H₂O panels of Fig. 7a. The poor convergence is accompanied by dipole response signals $\mu_{zzz}^{(3)}(t)$ that do not show the expected form. For example, the coefficient of determination for CH₄ ranges from $r^2 = 0.09$ to $r^2 = 0.22$ as the number of ramping cycles is increased.

The PW(2) approach produces $\gamma_{zzzz}^{\text{THG}}$ with small intersystem variations in error; the smallest error is 13% for HF, the largest 17.8% for H₂O. The properties also converge in a systematic fashion with increasing simula-

tion time. At the maximum simulation time, the PW(8) method is able to attain errors as small as -0.02% for HF and no larger than -0.25% for H₂O.

The QRCW approach produces $\gamma_{zzzz}^{\text{THG}}$ results with the smallest errors. The improvement over the other approaches is most striking when only a few optical cycles of simulation time are used. With QRCW (1,1), one gets $\gamma_{zzzz}^{\text{THG}}$ results with errors smaller than 1.6% for HF, H₂O and NH₃ and somewhat higher errors for Ne and CH₄. Including an extra ramping cycle, the QRCW(2,1) method reduces the errors of Ne from -17% to 3% and of CH₄ from -21% to 2.0%. Hence, the QRCW(2,1) method stands out as a possible compromise between computational cost and accuracy. The most accurate $\gamma_{zzzz}^{\text{THG}}$ results are acquired using the QRCW(7,1) method, achieving accuracies with errors below 0.8% for all systems. However, the lowest error obtained for $\gamma_{zzzz}^{\text{THG}}$ is still a thousandfold greater than that found for the polarizabilities and β_{zzzz}^{OR} , showing that some loss of accuracy

TABLE III: The degenerate four wave mixing component $\gamma_{jjjj}^{\text{DFWM}}$ of the second hyperpolarizabilities of Ne, HF, H₂O, NH₃ and CH₄ extracted from TDCCSD, TDOMP2, TDCC2, and TDCIS simulations compared with results from cubic response theory.

	TDCCSD	TDOMP2	TDCC2	TDCIS		TDCCSD	TDOMP2	TDCC2	TDCIS	
HF	$\gamma_{xxxx}^{\text{DFWM}}$					$\gamma_{zzzz}^{\text{DFWM}}$				
	PW(3)	-254	-284	-342	-109	-303	-312	-397	-184	
	LRCW(2,1)	-326	-360	-397	-134	-354	-334	-424	-219	
	QRCW(2,1)	-290	-324	-393	-128	-356	-365	-439	-215	
	Response	-298		-387	-128	-358		-441	-217	
NH ₃	$\gamma_{yyyy}^{\text{DFWM}}$					$\gamma_{zzzz}^{\text{DFWM}}$				
	PW(3)	-913	-955	-1050	64.2	-4940	-5550	-6100	-2690	
	LRCW(2,1)	-948	-1310	-1430	-71.9	-5900	-6540	-7350	-3240	
	QRCW(2,1)	-1100	-1140	-1260	73.9	-5930	-6570	-7230	-3190	
	Response	-1090		-1260	78.8	-5870		-7240	-3200	
H ₂ O	$\gamma_{xxxx}^{\text{DFWM}}$					$\gamma_{yyyy}^{\text{DFWM}}$				
	PW(3)	-1260	-1420	-1640	-590	-438	-449	-521	5.67	
	LRCW(2,1)	-1550	-1660	-1950	-715	-495	-681	-651	-44.3	
	QRCW(2,1)	-1510	-1690	-1950	-706	-522	-538	-621	4.39	
	Response	-1510		-1950	-703	-524		-623	7.44	
	$\gamma_{zzzz}^{\text{DFWM}}$									
	PW(3)	-803	-877	-1010	-349					
	LRCW(2,1)	-975	-1010	-1180	-431					
	QRCW(2,1)	-963	-1050	-1200	-419					
	Response	-959		-1200	-417					
Ne	$\gamma_{jjjj}^{\text{DFWM}}$				CH ₄	$\gamma_{jjjj}^{\text{DFWM}}$				
	PW(3)	-79.3	-84.7	-95.7		-41.8	-1730	-1750	-1870	313
	LRCW(2,1)	-80.6	-114	-105		-51.3	-2330	-2130	-2500	192
	QRCW(2,1)	-93.1	-99.7	-114		-50.4	-2030	-2080	-2200	373
	Response	-94.2		-114		-49.7	-2050		-2210	384

must be expected for higher-order responses.

The extracted $\gamma_{zzzz}^{\text{DFWM}}$ results behave similarly to $\gamma_{zzzz}^{\text{THG}}$. The errors are generally large when two cycles of simulation time is used, 20% for LRCW(1,1), 31% for PW(2), and -6.7% for QRCW(1,1). Increasing the simulation time quickly leads to very accurate results when using the QRCW approach, less so for the PW approach, and the LRCW approach continues to perform irregularly as a function of simulation time. The main difference between the $\gamma_{zzzz}^{\text{DFWM}}$ and the $\gamma_{zzzz}^{\text{THG}}$ results lies in the slower convergence with increasing simulation time for the PW approach. The inferior performance of PW for $\gamma_{zzzz}^{\text{DFWM}}$ resembles the poorer performance found for β^{SHG} . The $\gamma_{zzzz}^{\text{DFWM}}$ results are accurate to within 0.3% for all systems when using the QRCW(7,1) approach.

Also, for the second hyperpolarizability we find a relation between r^2 values of the fit with the errors observed, confirming that r^2 values close to 1 are needed for a reliable extraction. The results obtained with the TDCCSD, TDOMP2, TDCC2, and TDCIS methods for $\gamma_{xxxx}^{\text{THG}}$, $\gamma_{yyyy}^{\text{THG}}$, and $\gamma_{zzzz}^{\text{THG}}$ after a total simulation time of

three optical cycles are shown in Table II. The $\gamma_{xxxx}^{\text{DFWM}}$, $\gamma_{yyyy}^{\text{DFWM}}$, and $\gamma_{zzzz}^{\text{DFWM}}$ results are shown in Table III. In general, we observe that the QRCW(2,1) approach yields more accurate second hyperpolarizabilities than the LRCW(2,1) and PW(3) approaches regardless of the electronic-structure method used. We note in passing that, in agreement with the observations made in Ref. 15, the TDOMP2 method yields optical properties that fall between those of the TDCC2 and TDCCSD methods. Although there is no response data available for the OMP2 method, we may assume that the TDOMP2 values reported with the QRCW approach is correct to within 1% based on the accuracies observed for the TDCCSD, TDCC2, and TDCIS methods.

As expected,⁴⁴ the simulations at the TDCIS level provides optical properties vastly different from the other three methods due to lack of electron correlation. Since the fourth-order dipole signal is very weak, separation by numerical differentiation is more challenging. Although the optimal choice of the electric-field strength is beyond the scope of this paper, we remark that increasing the

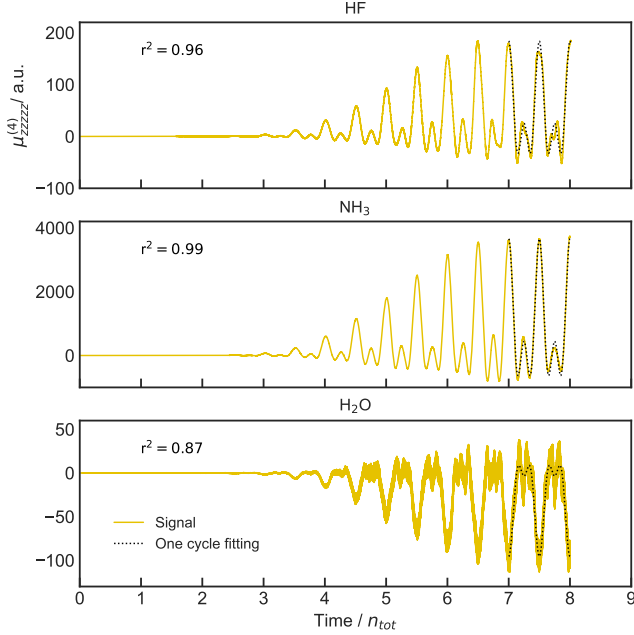


FIG. 8: The fourth-order dipole response functions obtained from TDCCSD simulations for the HF, NH_3 and H_2O molecules using QRCW(7,1).

TABLE IV: The third hyperpolarizabilities δ_{zzzzz} extracted from TDCCSD simulations with QRCW(2,1), QRCW(7,1), PW(3) and PW(8).

		$\delta_{zzzzz}^{\text{FHG}}$	$\delta_{zzzzz}^{\text{HSHG}}$	$\delta_{zzzzz}^{\text{HOR}}$
HF	QRCW(2,1)	10 636	3 863	2 726
	QRCW(7,1)	11 948	3 808	2 705
	PW(3)	14 795	3 082	2 641
	PW(8)	12 512	3 699	2 724
NH_3	QRCW(2,1)	324 317	76 998	56 012
	QRCW(7,1)	231 482	81 326	53 906
	PW(3)	244 356	62 355	52 571
	PW(8)	240 228	74 587	54 103
H_2O	QRCW(2,1)	-5 067	-2 271	-1 694
	QRCW(7,1)	-4 520	-2 208	-1 662
	PW(3)	-4 452	-1 748	-1 608
	PW(8)	-4 536	-2 129	-1 665

electric-field strength from $E = 0.001$ to $E = 0.004$ seems to reduce the error of the numerical differentiation for the TDCIS method.

E. Third hyperpolarizability

The RCW and PW approaches can straightforwardly be extended to evaluate higher order properties, here ex-

emplified with third hyperpolarizabilities. An example of extracting fourth hyperpolarizabilities can be found in the supplementary material.

To the best of our knowledge, there are no implemented analytic response functions available for third hyperpolarizabilities. Instead, we will use the r^2 value of the fit to the fourth-order dipole response function $\mu^{(4)}(t)$ to gauge the accuracy of the extracted third hyperpolarizabilities. Figure 8 shows $\mu_{zzzzz}^{(4)}(t)$ calculated at the TDCCSD level of theory along with the associated curve fitting using the QRCW(7,1) method. The fitted curves have r^2 values ranging from 0.87 to 0.99, indicating that only the third hyperpolarizability results for NH_3 ($r^2 = 0.99$) and HF ($r^2 = 0.96$) are fully reliable while the results for H_2O are decent estimates.

The third hyperpolarizabilities for HF, NH_3 , and H_2O are given in Table IV. The discrepancies between the PW and RCW approaches are modest, typically on the order of 3% for the $\delta_{zzzzz}^{\text{FHG}}$ and 0.5% for the $\delta_{zzzzz}^{\text{HSHG}}$ when simulating for a total of eight optical cycles. Increasing the total simulation time (i.e., increasing n_r in the case of the QRCW approach) is likely to improve the accuracy further, in analogy to the convergence behavior observed for the lower-order responses above.

V. CONCLUDING REMARKS

We have compared three approaches to the extraction of linear and nonlinear optical properties from electron dynamics simulations with respect to accuracy relative to results from response theory and computational effort. The LRCW and QRCW approaches are based on a monochromatic continuous wave perturbation ramped from zero to full strength linearly and quadratically, while the PW approach uses Fourier filtering to extract properties at a given frequency from signals recorded during the interaction of electrons with a finite laser pulse. All three approaches rely on numerical (finite-difference) differentiation to separate different orders of response in the time domain, followed by curve fitting to obtain the property of interest at a given frequency.

Showing irregular convergence behavior towards response results as the ramping time is increased, the LRCW approach is difficult to apply reliably for higher-order nonlinear responses. Using a single optical cycle for ramping, as previously recommended,⁶ is found to be insufficient. On the other hand, we find that the post-ramp simulation time can be reduced to a single cycle without incurring an accuracy penalty, as opposed to the four ramping cycles proposed by Ding *et al.*⁶

The QRCW approach, proposed in this work, is a clear improvement due to reduced nonadiabatic effects. Although the convergence behavior remains somewhat irregular, errors observed for linear and nonlinear response properties are significantly reduced. Our tests indicate that the QRCW approach yields highly accurate linear and quadratic response properties with simulation times

as short as two optical cycles, one cycle for ramping and one post-ramp cycle for extracting the response property of interest. An additional ramp cycle should be added to reliably extract cubic response properties, however. The QRCW approach thus yields significantly improved accuracy at about half the computational cost of the LRCW approach as proposed by Ding *et al.*⁶

We find that the coefficient of determination (r^2) obtained for the curve fitting can be used as an indicator of accuracy in lieu of analytical results from response theory. In all cases studied in this work, the r^2 value can be improved by increasing the ramping time of the QRCW approach.

The PW approach offers an alternative to QRCW. The PW approach shows monotonous but typically rather slow convergence towards response results with respect to simulation time. For comparable accuracy, the PW approach typically requires much longer simulation times than the QRCW approach, which we recommend for reliable and efficient extraction of linear and nonlinear response properties.

While our tests are based on TDCC and TDCIS methods, we expect that our conclusions remain valid also for other electronic-structure methods such as real-time time-dependent density-functional theory.

SUPPLEMENTARY MATERIAL

The HF, H₂O, NH₃, and CH₄ geometries used throughout this article can be found in section I of the supplementary material. The procedure for finding the fifth-order hyperpolarizabilities and example calculations for the HF molecule are found in section II. Tables displaying polarizabilities, first hyperpolarizabilities, and second hyperpolarizabilities extracted using QRCW(7,1), LRCW(7,1), and PW(8) for all unique diagonal directions at the CC2, OMP2, CIS, and CCSD levels of theory are available in section III. Finally, figures displaying the relative errors of the polarizabilities, first hyperpolarizabilities, and second hyperpolarizabilities as functions of $n_{tot} = (2, 3, 4, 5, 6, 7, 8)$ at the CC2 and CCSD levels of theory for all diagonal directions are available in section IV.

ACKNOWLEDGMENT

This work was supported by the Research Council of Norway through its Centres of Excellence scheme, project number 262695. The calculations were performed on resources provided by Sigma2—the National Infrastructure for High Performance Computing and Data Storage in Norway, Grant No. NN4654K. S. K. and T. B. P. acknowledge the support of the Centre for Advanced Study in Oslo, Norway, which funded and hosted the CAS research project *Attosecond Quantum Dynamics Beyond*

the Born-Oppenheimer Approximation during the academic year 2021-2022.

DATA AVAILABILITY STATEMENT

The data that support the findings of this study are available from the corresponding author upon reasonable request.

- ¹K. Yabana and G. F. Bertsch, “Time-dependent local-density approximation in real time,” *Phys. Rev. B* **54**, 4484–4487 (1996).
- ²A. Argyrios Tsolakidis, D. Sánchez-Portal, and R. M. Martin, “Calculation of the optical response of atomic clusters using time-dependent density functional theory and local orbitals,” *Phys. Rev. B* **66**, 235416 (2002).
- ³K. Yabana, T. Nakatsukasa, J.-I. Iwata, and G. F. Bertsch, “Real-time, real-space implementation of the linear response time-dependent density-functional theory,” *Phys. Status Solidi B* **243**, 1121–1138 (2006).
- ⁴F. Wang, C. Y. Yam, G. Chen, and K. Fan, “Density matrix based time-dependent density functional theory and the solution of its linear response in real time domain,” *J. Chem. Phys.* **126**, 134104 (2007).
- ⁵F. Wang, C. Y. Yam, and G. Chen, “Time-dependent density-functional theory/localized density matrix method for dynamic hyperpolarizability,” *J. Chem. Phys.* **126**, 244102 (2007).
- ⁶F. Ding, B. E. Van Kuiken, B. E. Eichinger, and X. Li, “An efficient method for calculating dynamical hyperpolarizabilities using real-time time-dependent density functional theory,” *J. Chem. Phys.* **138**, 064104 (2013).
- ⁷M. Yamaguchi and K. Nobusada, “Large Hyperpolarizabilities of the Second Harmonic Generation Induced by Nonuniform Optical Near Fields,” *J. Phys. Chem. C* **120**, 23748–23755 (2016).
- ⁸L. Konecny, M. Kadek, S. Komorovsky, O. L. Malkina, K. Ruud, and M. Repisky, “Acceleration of Relativistic Electron Dynamics by Means of X2C Transformation: Application to the Calculation of Nonlinear Optical Properties,” *J. Chem. Theory Comput.* **12**, 5823–5833 (2016).
- ⁹T. Yatsui, M. Yamaguchi, and K. Nobusada, “Nano-scale chemical reactions based on non-uniform optical near-fields and their applications,” *Prog. Quantum Electron.* **55**, 166–194 (2017).
- ¹⁰P. J. Lestrange, M. R. Hoffmann, and X. Li, “Time-Dependent Configuration Interaction Using the Graphical Unitary Group Approach: Nonlinear Electric Properties,” in *Advances in Quantum Chemistry*, Novel Electronic Structure Theory: General Innovations and Strongly Correlated Systems, Vol. 76, edited by P. E. Hoggan (Academic Press, 2018) pp. 295–313.
- ¹¹J. J. Goings, P. J. Lestrange, and X. Li, “Real-time time-dependent electronic structure theory,” *WIREs Comput. Mol. Sci.* **8**, e1341 (2018).
- ¹²M. Uemoto, Y. Kuwabara, S. A. Sato, and K. Yabana, “Nonlinear polarization evolution using time-dependent density functional theory,” *J. Chem. Phys.* **150**, 094101 (2019).
- ¹³X. Li, N. Govind, C. Isborn, A. E. DePrince, and K. Lopata, “Real-Time Time-Dependent Electronic Structure Theory,” *Chem. Rev.* **120**, 9951–9993 (2020).
- ¹⁴A. Baiardi, “Electron Dynamics with the Time-Dependent Density Matrix Renormalization Group,” *J. Chem. Theory Comput.* **17**, 3320–3334 (2021).
- ¹⁵H. E. Kristiansen, B. S. Ofstad, E. Hauge, E. Aurbakken, Ø. S. Schøyen, S. Kvaal, and T. B. Pedersen, “Linear and Nonlinear Optical Properties from TDOMP2 Theory,” *J. Chem. Theory Comput.* **18**, 3687–3702 (2022).
- ¹⁶H. E. Kristiansen, B. S. Ofstad, E. Hauge, E. Aurbakken, Ø. S. Schøyen, S. Kvaal, and T. B. Pedersen, “Correction to “Linear and Nonlinear Optical Properties from TDOMP2 Theory,”” *J. Chem. Theory Comput.* **18**, 5755–5757 (2022).

- ¹⁷J. Olsen and P. Jørgensen, "Linear and nonlinear response functions for an exact state and for an MCSCF state," *J. Chem. Phys.* **82**, 3235–3264 (1985).
- ¹⁸O. Christiansen, P. Jørgensen, and C. Hättig, "Response functions from Fourier component variational perturbation theory applied to a time-averaged quasienergy," *Int. J. Quantum Chem.* **68**, 1–52 (1998).
- ¹⁹P. N. Butcher and D. Cotter, *The Elements of Nonlinear Optics*, Cambridge Studies in Modern Optics (Cambridge University Press, Cambridge, 1990).
- ²⁰T. Helgaker, S. Coriani, P. Jørgensen, K. Kristensen, J. Olsen, and K. Ruud, "Recent Advances in Wave Function-Based Methods of Molecular-Property Calculations," *Chem. Rev.* **112**, 543–631 (2012).
- ²¹S. Hermanns, K. Balzer, and M. Bonitz, "The non-equilibrium Green function approach to inhomogeneous quantum many-body systems using the generalized Kadanoff–Baym ansatz," *Phys. Scr.* **T151**, 014036 (2012).
- ²²I. Barth and C. Lasser, "Trigonometric pulse envelopes for laser-induced quantum dynamics," *J. Phys. B* **42**, 235101 (2009).
- ²³J. B. Foresman, M. Head-Gordon, J. A. Pople, and M. J. Frisch, "Toward a systematic molecular orbital theory for excited states," *J. Phys. Chem.* **96**, 135–149 (1992).
- ²⁴T. Klamroth, "Laser-driven electron transfer through metal-insulator-metal contacts: Time-dependent configuration interaction singles calculations for a jellium model," *Phys. Rev. B* **68**, 245421 (2003).
- ²⁵T. B. Pedersen and S. Kvaal, "Symplectic integration and physical interpretation of time-dependent coupled-cluster theory," *J. Chem. Phys.* **150**, 144106 (2019).
- ²⁶O. Christiansen, H. Koch, and P. Jørgensen, "The second-order approximate coupled cluster singles and doubles model CC2," *Chem. Phys. Lett.* **243**, 409–418 (1995).
- ²⁷H. Pathak, T. Sato, and K. L. Ishikawa, "Time-dependent optimized coupled-cluster method for multielectron dynamics. III. A second-order many-body perturbation approximation," *J. Chem. Phys.* **153**, 034110 (2020).
- ²⁸T. B. Pedersen and H. Koch, "Coupled cluster response functions revisited," *J. Chem. Phys.* **106**, 8059–8072 (1997).
- ²⁹D. E. Woon and T. H. Dunning, "Gaussian basis sets for use in correlated molecular calculations. IV. Calculation of static electrical response properties," *J. Chem. Phys.* **100**, 2975–2988 (1994).
- ³⁰R. A. Kendall, T. H. Dunning, and R. J. Harrison, "Electron affinities of the first-row atoms revisited. Systematic basis sets and wave functions," *J. Chem. Phys.* **96**, 6796–6806 (1992).
- ³¹B. P. Pritchard, D. Altarawy, B. Didier, T. D. Gibson, and T. L. Windus, "New Basis Set Exchange: An Open, Up-to-Date Resource for the Molecular Sciences Community," *J. Chem. Inf. Model.* **59**, 4814–4820 (2019).
- ³²Q. Sun, T. C. Berkelbach, N. S. Blunt, G. H. Booth, S. Guo, Z. Li, J. Liu, J. D. McClain, E. R. Sayfutyarova, S. Sharma, S. Wouters, and G. K. L. Chan, "PySCF: the Python-based simulations of chemistry framework," *WIREs Comput. Mol. Sci.* **8**, e1340 (2018).
- ³³Aurbakken, E. and Kristiansen H. E., and Kvaal, S. and Ofstad, B. S. and Pedersen, T. B. and Schøyen, Ø. S., "HyQD," (2023-02-04), URL: <https://github.com/HyQD>.
- ³⁴E. Hairer, G. Wanner, and C. Lubich, "Geometric numerical integration," in *Springer Series in Computational Mathematics*, Vol. 31 (Springer, Berlin, Heidelberg, 2006) 2nd ed.
- ³⁵P. Virtanen, R. Gommers, T. E. Oliphant, M. Haberland, T. Reddy, D. Cournapeau, E. Burovski, P. Peterson, W. Weckesser, J. Bright, S. J. van der Walt, M. Brett, J. Wilson, K. J. Millman, N. Mayorov, A. R. J. Nelson, E. Jones, R. Kern, E. Larson, C. J. Carey, Í. Polat, Y. Feng, E. W. Moore, J. VanderPlas, D. Laxalde, J. Perktold, R. Cimrman, I. Henriksen, E. A. Quintero, C. R. Harris, A. M. Archibald, A. H. Ribeiro, F. Pedregosa, P. van Mulbregt, and SciPy 1.0 Contributors, "SciPy 1.0: Fundamental Algorithms for Scientific Computing in Python," *Nat. Methods* **17**, 261–272 (2020).
- ³⁶K. Aidas, C. Angeli, K. L. Bak, V. Bakken, R. Bast, L. Boman, O. Christiansen, R. Cimiraglia, S. Coriani, P. Dahle, E. K. Dalskov, U. Ekström, T. Enevoldsen, J. J. Eriksen, P. Ettenhuber, B. Fernández, L. Ferrighi, H. Fliegl, L. Frediani, K. Hald, A. Halkier, C. Hättig, H. Heiberg, T. Helgaker, A. C. Hennum, H. Hettema, E. Hjertenaes, S. Høst, I.-M. Høyvik, M. F. Iozzi, B. Jansík, H. J. A. Jensen, D. Jonsson, P. Jørgensen, J. Kauczor, S. Kirpekar, T. Kjaergaard, W. Klopper, S. Knecht, R. Kobayashi, H. Koch, J. Kongsted, A. Krapp, K. Kristensen, A. Ligabue, O. B. Lutnaes, J. I. Melo, K. V. Mikkelsen, R. H. Myhre, C. Neiss, C. B. Nielsen, P. Norman, J. Olsen, J. M. H. Olsen, A. Osted, M. J. Packer, P. Pawłowski, T. B. Pedersen, P. F. Provasi, S. Reine, Z. Rinkevicius, T. A. Ruden, K. Ruud, V. V. Rybkin, P. Salek, C. C. M. Samson, A. Sánchez de Merás, T. Saue, S. P. A. Sauer, B. Schimmelpfennig, K. Snedkov, A. H. Steindal, K. O. Sylvester-Hvid, P. R. Taylor, A. M. Teale, E. I. Tellgren, D. P. Tew, A. J. Thorvaldsen, L. Thøgersen, O. Vahtras, M. A. Watson, D. J. D. Wilson, M. Ziolkowski, and H. Ågren, "The Dalton quantum chemistry program system," *WIREs Comput. Mol. Sci.* **4**, 269–284 (2014).
- ³⁷J. M. H. Olsen, S. Reine, O. Vahtras, E. Kjellgren, P. Reinholdt, K. O. Hjørth Dundas, X. Li, J. Cukras, M. Ringholm, E. D. Hedegård, R. Di Remigio, N. H. List, R. Faber, B. N. Cabral Tenorio, R. Bast, T. B. Pedersen, Z. Rinkevicius, S. P. A. Sauer, K. V. Mikkelsen, J. Kongsted, S. Coriani, K. Ruud, T. Helgaker, H. J. A. Jensen, and P. Norman, "Dalton Project: A Python platform for molecular- and electronic-structure simulations of complex systems," *J. Chem. Phys.* **152**, 214115 (2020).
- ³⁸H. Koch, A. Sánchez De Merás, T. Helgaker, and O. Christiansen, "The integral-direct coupled cluster singles and doubles model," *J. Chem. Phys.* **104**, 4157–4165 (1996).
- ³⁹A. Halkier, H. Koch, O. Christiansen, P. Jørgensen, and T. Helgaker, "First-order one-electron properties in the integral-direct coupled cluster singles and doubles model," *J. Chem. Phys.* **107**, 849–866 (1997).
- ⁴⁰O. Christiansen, A. Halkier, H. Koch, P. Jørgensen, and T. Helgaker, "Integral-direct coupled cluster calculations of frequency-dependent polarizabilities, transition probabilities, and excited-state properties," *J. Chem. Phys.* **108**, 2801–2816 (1998).
- ⁴¹C. Hättig, O. Christiansen, H. Koch, and P. Jørgensen, "Frequency-dependent first hyperpolarizabilities using coupled cluster quadratic response theory," *Chem. Phys. Lett.* **269**, 428–434 (1997).
- ⁴²C. Hättig, O. Christiansen, and P. Jørgensen, "Frequency-dependent second hyperpolarizabilities using coupled cluster cubic response theory," *Chem. Phys. Lett.* **269**, 139–146 (1998).
- ⁴³B. J. Orr and J. F. Ward, "Perturbation theory of the non-linear optical polarization of an isolated system," *Mol. Phys.* **20**, 513–526 (1971).
- ⁴⁴H. Larsen, J. Olsen, C. Hättig, P. Jørgensen, O. Christiansen, and J. Gauss, "Polarizabilities and first hyperpolarizabilities of HF, Ne, and BH from full configuration interaction and coupled cluster calculations," *J. Chem. Phys.* **111**, 1917–1925 (1999).

Supplementary material for “Adiabatic extraction of nonlinear optical properties from real-time time-dependent electronic-structure theory”

Benedicte Sverdrup Ofstad,^{1, a)} Håkon Emil Kristiansen,¹ Einar Aurbakken,¹ Øyvind Sigmundson Schøyen,² Simen Kvaal,¹ and Thomas Bondo Pedersen^{1, b)}

¹⁾*Hylleraas Centre for Quantum Molecular Sciences, Department of Chemistry, University of Oslo, Norway*

²⁾*Department of Physics, University of Oslo, Norway*

(Dated: 7 February 2023)

I. MOLECULAR GEOMETRIES

The molecular geometry input used for the calculations are displayed in Table I.

TABLE I: Cartesian coordinates in Bohr.

	x	y	z
Ne			
Ne	0	0	0
HF			
H	0	0	0
F	0	0	1.7328795
H ₂ O			
O	0	0	-0.1239093563
H	0	1.4299372840	0.9832657567
H	0	-1.4299372840	0.9832657567
NH ₃			
N	0	0	0.2010
H	0	1.7641	-0.4690
H	1.5277	-0.8820	-0.4690
H	-1.5277	-0.8820	-0.4690
CH ₄			
C	0	0	0
H	1.2005	1.2005	1.2005
H	-1.2005	-1.2005	1.2005
H	-1.2005	1.2005	-1.2005
H	1.2005	-1.2005	-1.2005

^{a)}Electronic mail: b.s.ofstad@kjemi.uio.no

^{b)}Electronic mail: t.b.pedersen@kjemi.uio.no

II. FOURTH HYPERPOLARIZABILITY

To obtain the fourth hyperpolarizability, the time-dependent dipole moment is expanded to fifth order

$$\begin{aligned} \mu_i(t) = & \mu_i(0) + \sum_j \mu_{ij}^{(1)}(t) \mathcal{E}_j + \sum_{jk} \mu_{ijk}^{(2)}(t) \mathcal{E}_j \mathcal{E}_k + \sum_{jkl} \mu_{ijkl}^{(3)}(t) \mathcal{E}_j \mathcal{E}_k \mathcal{E}_l \\ & + \sum_{jklm} \mu_{ijklm}^{(4)}(t) \mathcal{E}_j \mathcal{E}_k \mathcal{E}_l \mathcal{E}_m + \sum_{jklmn} \mu_{ijklmn}^{(5)}(t) \mathcal{E}_j \mathcal{E}_k \mathcal{E}_l \mathcal{E}_m \mathcal{E}_n + \dots \end{aligned} \quad (1)$$

The central difference formula for extracting $\mu_{ijjjjj}^{(5)}(t)$ is

$$\mu_{ijjjjj}^{(5)}(t) = \frac{29\Delta_i^-(t; \mathcal{E}_j) - 26\Delta_i^-(t; 2\mathcal{E}_j) + 9\Delta_i^-(t; 3\mathcal{E}_j) - \Delta_i^-(t; 4\mathcal{E}_j)}{720\mathcal{E}_j^5} + O(\mathcal{E}_j^4). \quad (2)$$

The quintic response is given by

$$\begin{aligned} \mu_{ijjjjj}^{(5)}(t) = & \frac{1}{120} \iiint\limits_{-\infty}^{\infty} \epsilon_{ijjjjj}(-\omega^{(5)}; \omega_1, \omega_2, \omega_3, \omega_4, \omega_5) \\ & \times \tilde{F}(\omega_1) \tilde{F}(\omega_2) \tilde{F}(\omega_3) \tilde{F}(\omega_4) \tilde{F}(\omega_5) e^{-i(\omega_1 + \omega_2 + \omega_3 + \omega_4 + \omega_5)t} \\ & \times d\omega_1 d\omega_2 d\omega_3 d\omega_4 d\omega_5. \end{aligned} \quad (3)$$

With $F(t) = \cos(\omega t)$, one obtains

$$\begin{aligned} \mu_{ijjjjj}^{(5)}(t) = & \frac{1}{1920} [\epsilon_{ijjjjj}(-5\omega; \omega, \omega, \omega, \omega, \omega) \cos(5\omega t) \\ & + 5\epsilon_{ijjjjj}(-3\omega; \omega, \omega, \omega, \omega, -\omega) \cos(3\omega t) \\ & + 10\epsilon_{ijjjjj}(-\omega; \omega, \omega, \omega, -\omega, -\omega) \cos(\omega t)] \\ = & [\epsilon_{ijjjjj}^{\text{5HG}}(\omega) \cos(5\omega t) \\ & + 5\epsilon_{ijjjjj}^{\text{HTHG}}(\omega) \cos(3\omega t) \\ & + 10\epsilon_{ijjjjj}^{\text{D6WM}}(\omega) \cos(\omega t)]. \end{aligned} \quad (4)$$

For the HF molecule, we use $\omega = 0.05$, which is below one fourth of the first excitation energy. The fifth-order dipole signals extracted with the RCW and PW approaches are plotted in Figs. **1a** and **1b**, respectively, along with the least-squares fits and their r^2 values. The correlation for the fourth hyperpolarizability is reasonably good in the diagonal x -direction but very poor in the diagonal z -direction. This *might* be caused by instabilities in the numerical differentiation, Eq. (2), for which we have not studied convergence with respect to field strength. The results for the HF molecule in the x -direction are given in Table **II**. The PW and QRCW values agree to within 8%.

TABLE II: The $\epsilon^{5\text{HG}}$, ϵ^{HTHG} , and ϵ^{D6WM} component in the diagonal x - and y - direction of the fourth hyperpolarizability is extracted for the HF molecule at the CCSD level

	ω	$\epsilon_{xxxxx}^{5\text{HG}}$	$\epsilon_{xxxxx}^{\text{HTHG}}$	$\epsilon_{xxxxx}^{\text{D6WM}}$	$\epsilon_{zzzzzz}^{5\text{HG}}$	$\epsilon_{zzzzzz}^{\text{HTHG}}$	$\epsilon_{zzzzzz}^{\text{D6WM}}$
HF							
QRCW(7,1)	0.05	216238	135160	106098	408 000	183 000	142 000
PW(8)	0.05	234506	137296	102577	203 365	146 188	119 526

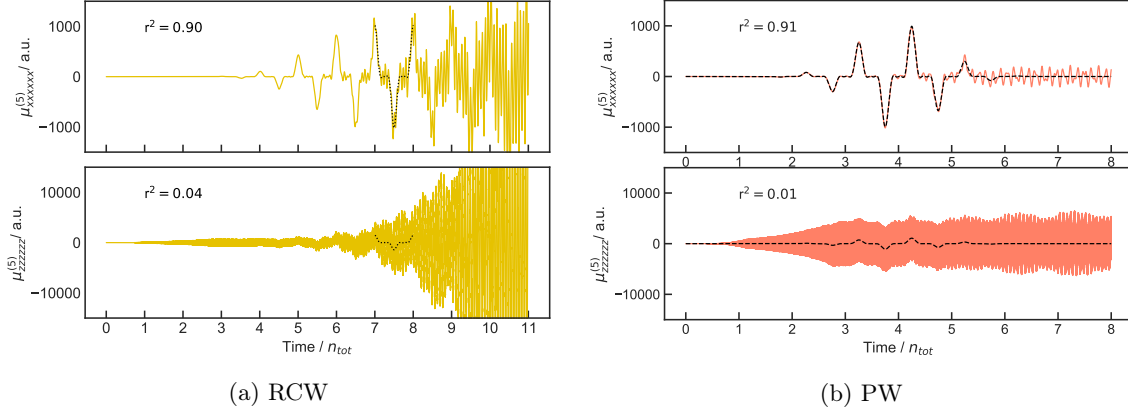


FIG. 1: The fifth-order dipole response obtained from TDCCSD simulations for HF using $n_r = 7$ quadratic ramp cycles followed by $n_p = 1$ post-ramp cycles in **1a** and $n_{\text{tot}} = 8$ pulsed wave cycles in **1b**.

III. POLARIZABILITIES AND FIRST HYPERPOLARIZABILITIES FROM TDCCSD, TDMP2, TDCC2, AND TDCIS SIMULATIONS

All unique diagonal cartesian components are presented for the polarizabilities in Table III and for the first hyperpolarizabilities in Table IV after a total of two optical cycles for the LRCW(1,1), QRCW(1,1) and PW(2) approach.

TABLE III: Polarizabilities

		TDCCSD	TDOMP2	TDCC2	TDCIS	TDCCSD	TDOMP2	TDCC2	TDCIS
HF		α_{xx}				α_{zz}			
	PW(2)	4.4534	4.5696	4.7192	4.2274	6.4199	6.5036	6.7898	6.4934
	LRCW(1,1)	4.4450	4.5657	4.7210	4.2238	6.4159	6.4913	6.7752	6.4884
	QRCW(1,1)	4.4405	4.5571	4.7077	4.2199	6.4080	6.4908	6.7757	6.4839
	Response	4.4419		4.7048	4.2208	6.4076		6.7759	6.4833
NH3		α_{yy}				α_{zz}			
	PW(2)	13.108	13.236	13.567	14.203	15.062	15.625	15.882	14.557
	LRCW(1,1)	13.105	13.233	13.564	14.199	15.077	15.615	15.879	14.553
	QRCW(1,1)	13.101	13.229	13.559	14.197	15.046	15.602	15.860	14.542
	Response	13.101		13.560	14.197	15.041		15.858	14.544
H2O		α_{xx}				α_{yy}			
	PW(2)	8.7901	9.1625	9.4244	8.1642	9.9359	10.063	10.436	10.461
	LRCW(1,1)	8.7941	9.1534	9.4151	8.1665	9.9337	10.059	10.433	10.461
	QRCW(1,1)	8.7810	9.1544	9.4161	8.1602	9.9318	10.058	10.431	10.457
	Response	8.7825		9.4150	8.1599	9.9318		10.431	10.458
		α_{zz}							
	PW(2)	9.1164	9.3398	9.6315	9.2544				
	LRCW(1,1)	9.1194	9.3342	9.6251	9.2557				
	QRCW(1,1)	9.1108	9.3343	9.6260	9.2507				
	Response	9.1114		9.6257	9.2506				
Ne		α_{jj}				α_{jj}			
	PW(2)	2.7392	2.7756	2.8592	2.5773	17.074	17.200	17.514	19.104
	LRCW(1,1)	2.7383	2.7743	2.8563	2.5747	17.055	17.184	17.495	19.095
	QRCW(1,1)	2.7363	2.7724	2.8558	2.5751	17.049	17.176	17.489	19.083
	Response	2.7364		2.8560	2.5752	17.050		17.490	19.081

TABLE IV: First hyperpolarizabilities

	TDCCSD	TDOMP2	TDCC2	TDCIS	TDCCSD	TDOMP2	TDCC2	TDCIS	
HF	β_{zzz}^{SHG}				β_{zzz}^{OR}				
	PW(2)	10.960	11.139	13.378	15.121	12.138	12.311	14.712	17.222
	LRCW(1,1)	14.295	14.702	17.832	19.774	12.816	13.066	15.676	18.177
	QRCW(1,1)	14.354	14.613	17.543	19.893	12.803	12.998	15.529	18.210
	Response	14.370		17.520	19.916	12.812		15.519	18.222
NH3	β_{yyy}^{SHG}				β_{yyy}^{OR}				
	PW(2)	-11.680	-12.202	-13.109	-11.828	-14.017	-14.611	-15.707	-14.291
	LRCW(1,1)	-15.782	-16.556	-17.817	-15.870	-15.032	-15.700	-16.894	-15.274
	QRCW(1,1)	-15.490	-16.160	-17.364	-15.719	-14.892	-15.511	-16.677	-15.200
	Response	-15.504		-17.397	-15.714	-14.898		-16.693	-15.198
	β_{zzz}^{SHG}				β_{zzz}^{OR}				
	PW(2)	21.531	27.849	30.677	23.919	22.742	29.020	32.178	27.590
	LRCW(1,1)	29.330	37.006	41.003	31.871	24.518	30.942	34.395	29.421
	QRCW(1,1)	27.944	36.114	39.798	31.643	23.859	30.445	33.764	29.271
	Response	28.020		39.869	31.558	23.904		33.801	29.228
H2O	β_{zzz}^{SHG}				β_{zzz}^{OR}				
	PW(2)	-7.2372	-7.8969	-9.9052	-13.725	-8.5816	-9.3123	-11.679	-16.687
	LRCW(1,1)	-9.6829	-10.483	-13.158	-18.271	-9.1759	-9.9075	-12.422	-17.782
	QRCW(1,1)	-9.5993	-10.479	-13.134	-18.239	-9.1164	-9.8935	-12.403	-17.752
	Response	-9.5909		-13.117	-18.247	-9.1119		-12.394	-17.756

IV. CONVERGENCE WITH RESPECT TO SIMULATION TIME

The full set of figures displaying the accuracy of the extracted property as a function of total simulation time are presented. All unique diagonal Cartesian components of the polarizabilities using the TDCC2 and TDCCSD method are presented in Fig. 2, the unique SHG and OR components of the first hyperpolarizabilities are presented in Fig. 3. The DFWM component of the second hyperpolarizability is presented in Fig. 4 and the THG component of the second hyperpolarizability is presented in Fig. 5.

The properties generated using the TDOMP2 method are not plotted due to lack of available response data, and the properties generated using the TDCIS method are not plotted due to lacking electron correlation which, in turn, renders the method unsuitable. The trends in the figures presented here are overall consistent with those presented and discussed in the main article.

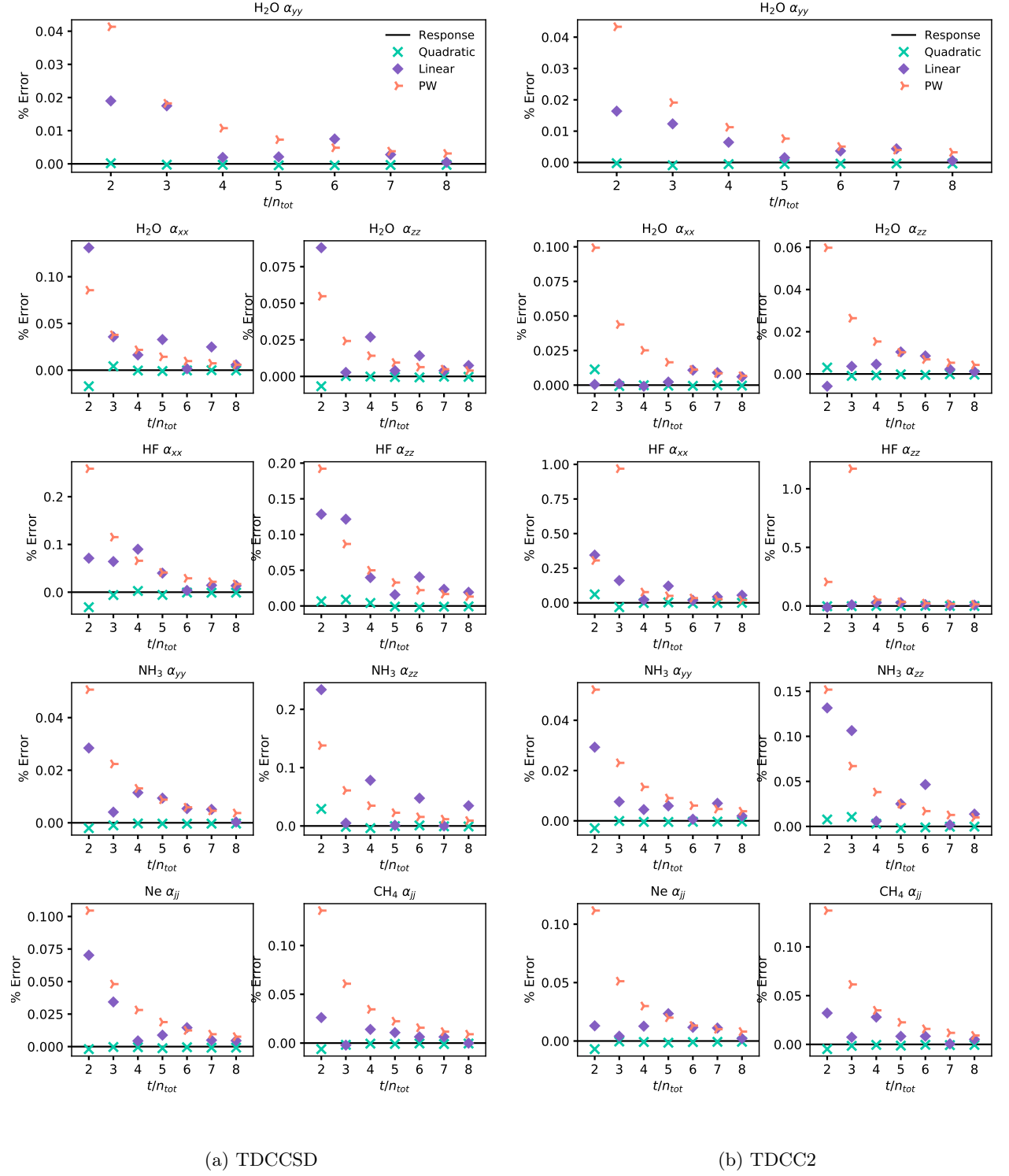


FIG. 2: The polarizability

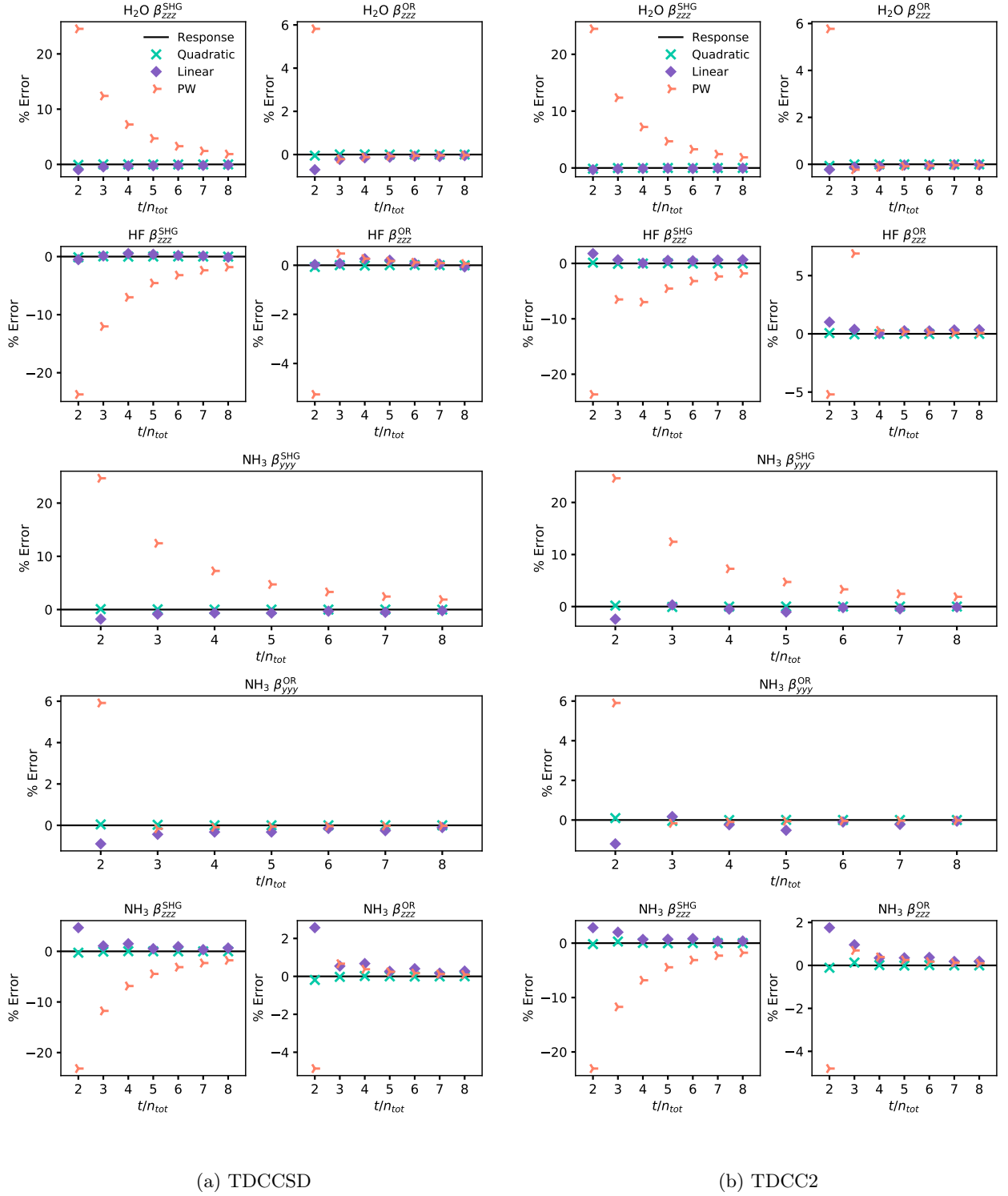


FIG. 3: The first hyperpolarizability

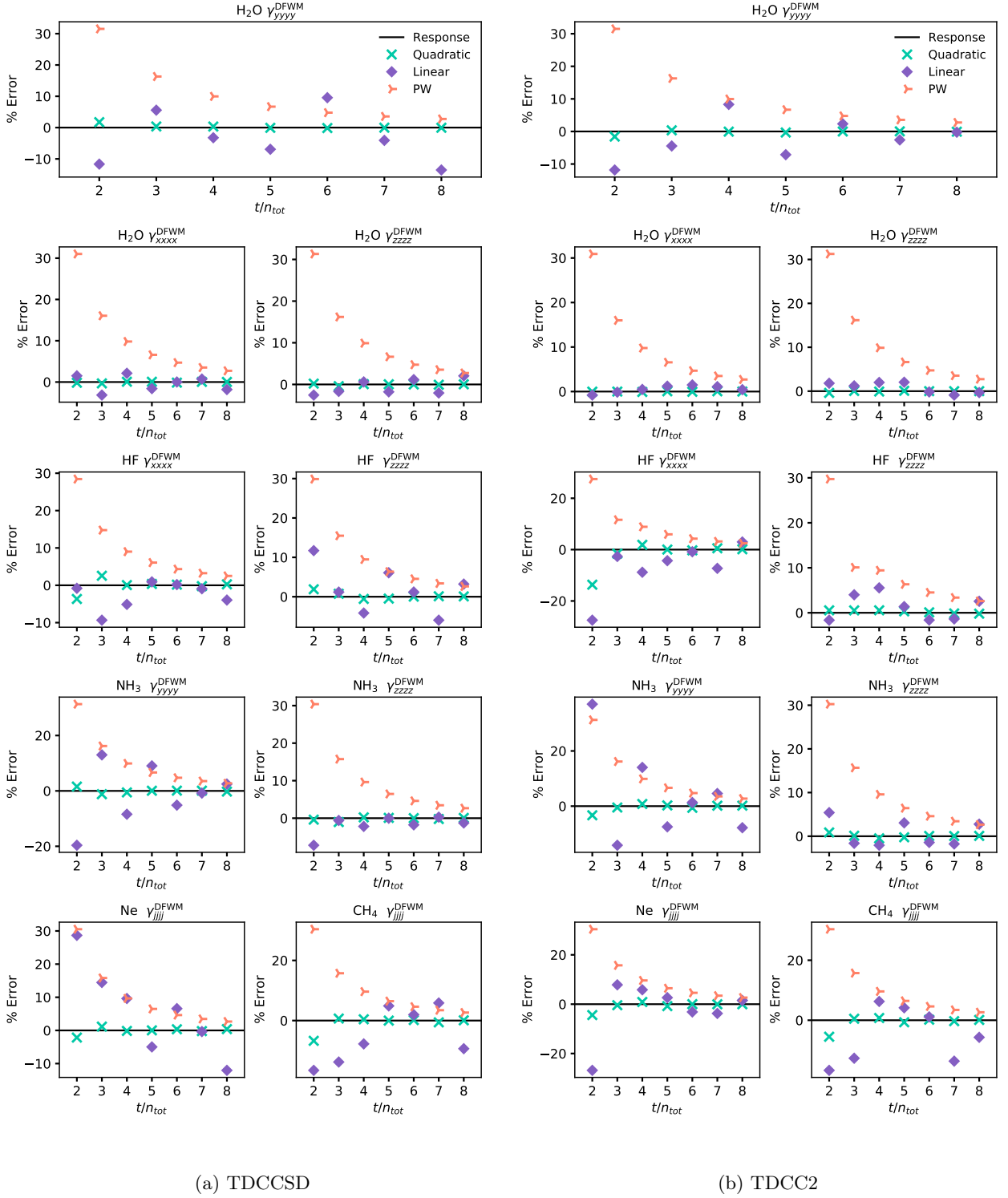


FIG. 4: The second hyperpolarizability DFWM

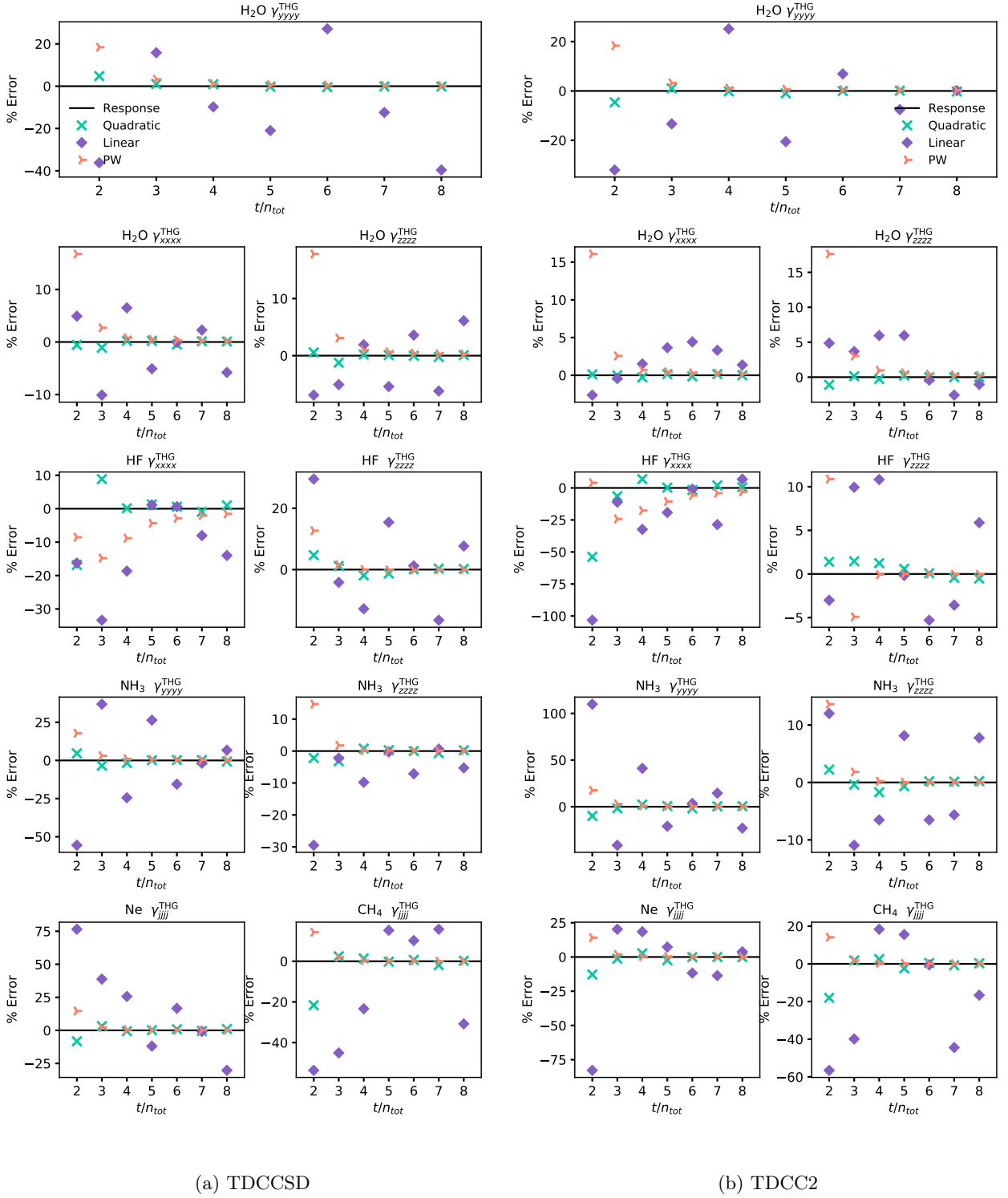


FIG. 5: The second hyperpolarizability THG